LBL-23551

Lawrence Berkeley Laboratory
UNIVERSITY OF CALIFORNIA

Presented at the Winter School on Physics,
Zakopane, Poland, May 1–8, 1987

HIGH-SPIN RESEARCH WITH HERA

R.M. Diamond

June 1987

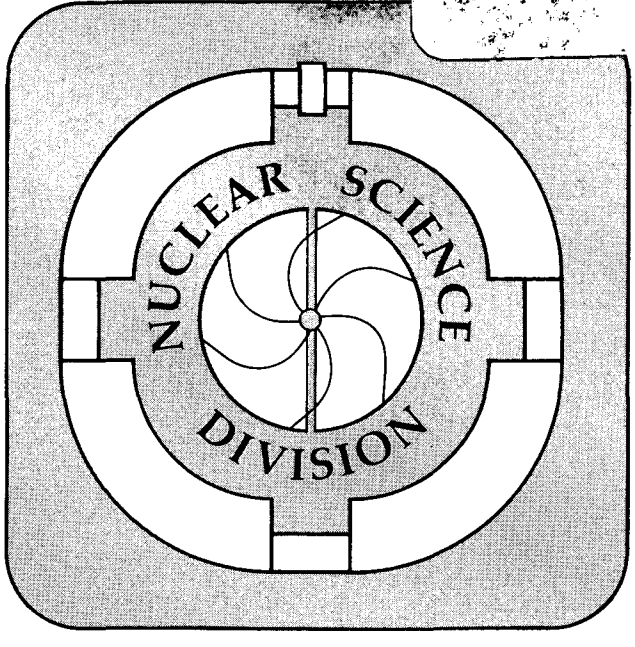

Prepared for the U.S. Department of Energy under Contract DE-AC03-76SF00098

LBL-23551

DISCLAIMER

LBL-23551

High-Spin Research with HERA

R.M. Diamond

Nuclear Science Division
Lawrence Berkeley Laboratory
University of California
Berkeley, California 94720

June 1987

This work was supported by the Director, Office of Energy Research, Division of Nuclear Physics of the Office of High Energy and Nuclear Physics of the U.S. Department of Energy under Contract DE-AC03-76SF00098.

High-Spin Research with HERA

R.M. Diamond

Nuclear Science Division
Lawrence Berkeley Laboratory
University of California
Berkeley, California 94720

I would very much like to thank the organizers of this workshop for not giving up on me, and it is a great pleasure to finally be here. It is always fun to see old friends again, and I feel that I know some of you (after two years) even though we have not met before.

My topic is high-spin research with HERA (High Energy-Resolution Array), our 21 Ge detector system, the first with bismuth germanate (BGO) Compton suppression. Before discussing some experiments with it, let me briefly describe the array.

HERA

As with many other types of spectroscopy , the limitations of in-beam nuclear spectroscopy usually involve energy resolution or statistics, or both. High resolution in γ-ray spectroscopy means Ge detectors. But they have a poor response function; for 1 MeV γ rays, ~1/4 go through a 5x5 cm Ge crystal (a "20%" detector), and only about 15% of the detected γ rays give a full-energy peak. This is bad enough for singles spectra, but means that only 2% of γ-γ coincidences are good (peak-peak) events, and a hopeless 0.3% of triple coincidences. A remedy was known; one must Compton suppress the Ge detectors. This had been done with sodium iodide (NaI) scintillators, but we decided in 1981 to try BGO,[1] as its greater density permitted more compact shields and thus allowed more detectors to be placed close together and closer

to the target. Since the companies were not able to produce single crystals of BGO large enough to make the Compton shields, we had the shields made of six pieces fitted together, each with its own photomultiplier tube. I believe most, if not all, such BGO shields made since then have been made in sections. Our arrangement is shown in Fig. 1, a co-axial design with a tapered front end to permit closer packing of the units; the taper roughly matches the energy of the back-scattered Compton γ rays. There are unprotected openings at the front and back ends. The back end is not so important to us, as it yields low-energy Compton γ rays, but even these can be greatly reduced by adding additional scintillators around a specially narrowed cold-finger for the Ge detector. But the front hole must be minimized, as it allows the Compton edges and high-energy Comptons to remain unsuppressed. We have reduced the size of this hole by the addition of NaI nose cones. Figure 2 shows the results for a ^{60}Co source. The peak/total ratio (above 300 keV) improves from ~20% to 50% with the BGO shield and to 55% with the NaI nose cone. Newer and bigger shields can give ratios as high as 60-70%, so tremendous improvement is possible. This makes a great difference in the proportion of "good" γ-γ events (from 2% to ~25%) and makes possible the use of triple coincidence events (~0.3% to 13%).

These units can be assembled to give 21 modules in three circles of seven each with the Ge detectors at a distance from the target as close as 15 cm. This distance is fixed by the touching of the shields, but there is also the necessity of holding the γ-ray summing to a small value (5% or less in our case) and even more importantly, of limiting the amount of Doppler broadening due to the finite acceptance angle of the Ge detectors, particularly those

near 90° to the beam direction. Figure 3 shows an artist's sketch in 1981 of the detector arrangement around a small central 4π ball of BGO sectors. The ball acts as a combined sum spectrometer and multiplicity filter, permitting cuts on the total excitation energy and on the γ-ray fold. Twelve of the Ge detector-BGO shield modules are shown in Fig. 4, and the next figure shows 15 of the units with their NaI nose cones attached; the remaining 6 units are pulled back out of the view of the camera.

The present status of the facility is that the 21 Ge detector-BGO shield units have been operating for ~2-1/2 years, and the additional NaI cones have been on for almost a year. The prototype BGO ball sectors have been tested and accepted, and the central ball should be complete in about 4 months. With the 21 detectors at 15 cm from the target, an event rate of 10^5/second (the order of our usual rate with a 1 mg/cm^2 target and a 2-3 pna beam in a ^{40}Ar,xn reaction), and an average γ-ray multiplicity of 20, we had estimated[1] and we have achieved three- and higher-fold coincidence rates of 2000/second. Up to now we have not stored double coincidences on tape as their ~10 K/second rate would yield too many tapes. But we now have a 4×10^6 word external memory into which we can put directly the γ-γ coincidences from all the detectors, as they are gain and zero-point adjusted to be the same. This arrangement will more than double the number of events in a 2000x2000 matrix used for initial spectral analyses.

Now I would like to tell you about some of the results we have obtained during the past year using this detector facility. I shall describe two types of studies: observation of superdeformation in the light Nd isotopes, and rotational damping at high spin and excitation energy in the continuum γ-ray

spectrum. My goal is not to impress you with how much we have learned, but rather to indicate how little we know and how much we have yet to understand.

Superdeformed Bands in the Light Rare-Earth Nuclei

Superdeformation originally meant states of very strongly deformed prolate nuclei with a 2:1 axis ratio, as first observed[2] in the spontaneously fissioning isomers near the ground state in certain Pu and Am nuclei. The large deformation was due to a second minimum in the potential-energy surface caused by a (several MeV) shell effect at that deformation.[3] Theoreticians predicted that such shell effects could produce secondary minima in the potential energy surfaces of nuclei in other regions of the Periodic Table, but stabilized only at high spins. (See ref. 4-12 for a partial listing.) The first example of an unusually strongly deformed, discrete-line band was observed[13] in ^{132}Ce, although the researchers were not able to link the members at the bottom of the band to the ground-state band, and the deformation was smaller, $\varepsilon \approx 0.35$ as derived from the moment of inertia, than that expected for a 2:1 axis ratio ($\varepsilon = 0.6$). A better value from limits set on the transition quadrupole moment by a Doppler-shift attenuation measurement[14] gave $\varepsilon \approx 0.4$. This is still less than that for a 2:1 axis ratio, but since the states involved appear to require a second minimum, the name "superdeformed" was generalized to include such a case. Here the origin of the second minimum is a weaker shell effect, but may also involve a liquid-drop effect predicted many years ago[15] that nuclei below about mass 150 at high spin would change to a strongly triaxial shape before fissioning at a still higher spin.

Then a year ago, a beautiful band extending from about spin 60$\hbar$ to 26$\hbar$

with a larger moment of inertia, suggesting $\varepsilon \sim 0.5$, was found[16] in ^{152}Dy, although again no links to the yrast band were seen. This case is the expected 2:1 band, or very close to it. But it does seem that the situation in the two mass regions is somewhat different, as in addition to the difference in the value of the deformation ε, the ^{152}Dy case is the only example in its mass region so far, while I want to describe our observation of strongly deformed bands, like the one in ^{132}Ce, superdeformed in the generalized sense but not 2:1, in ^{134}Nd, ^{135}Nd, and ^{136}Nd.

The first one observed[17] was in ^{135}Nd. It was produced by the ^{100}Mo(^{40}Ar,5n) reaction, at 173 and 177 MeV bombarding energy. The beam was provided by the LBL 88-Inch Cyclotron, and two thin foils (0.5 mg/cm^2) were stacked together as a target. The gains of the 21 Compton-suppressed Ge-detectors from the HERA array were matched on-line to compensate for the Doppler-shifts of the γ rays. The different angles of the detectors provided angular correlation information from which spin and parity assignments were made. A total of ~700 million three- and higher-fold events was recorded, of which approximately 25% came from the 5n channel. A two-dimensional array was produced from the data with $\sim 2 \times 10^9$ events, and then standard coincidence techniques were used to extract the less-deformed part of the level scheme of the nucleus, Fig. 6. Only a half-dozen states were known previously[18] in ^{135}Nd, but there is parallel work[19] which, as far as it goes, is basically in agreement with our study.

When the two-dimensional matrix had uncorrelated events removed by the method of ref. 20, ridges could be seen parallel to the diagonal of the array from ~900 keV to ~1600 keV. The spacing between the ridges is a measure

of the dynamic moment of inertia, $\mathcal{J}^{(2)}$, where $\mathcal{J}^{(2)}/\hbar^2 = dI/\hbar d\omega$ and $2\hbar\omega = E_\gamma$, the γ-ray transition energy. The value so determined of $\mathcal{J}^{(2)} \approx 60\hbar^2$ MeV^{-1} is almost 50% larger than the values for the ground-state and positive-parity bands, indicating the presence of superdeformed bands. For a first search, projections parallel to the diagonal (ridge cuts) at various distances (corresponding to different moments of inertia) in such a matrix were helpful to select candidates for discrete γ-ray energies belonging to a regularly spaced sequence with moment of inertia near that observed from the ridge separation. Then standard projections, parallel to an energy axis, were tried on the γ-ray energies at which peaks had appeared in the ridge cuts. In this way, a series of γ rays with an average energy spacing of 67.5 keV was found, leading to the superdeformed band depicted in Fig. 6. At its bottom, where the lowest in-band transitions gather approximately 10% of the reaction events leading to ^{135}Nd, this band branches out in many pathways, each carrying less than 1-2% intensity. This behavior indicates already that the structure of this band is very different from that of the other low-lying bands in the nucleus, since it does not decay preferentially to a particular state (with most similar configuration). To obtain a clean spectrum of this band, the triples data were sorted in a special way. Two gates were required, one on an in-band transition, the other either in-band or on a low-lying state seen in coincidence with the band in single-gated spectra. Figure 7 shows a background-subtracted spectrum of the third γ ray in coincidence with these double gates where we have summed the clean-gate combinations. All the lines in this double-coincidence spectrum come from ^{135}Nd and are related to the

superdeformed band. We are reasonably confident of one depopulation path (the 620 keV - 1184 keV sequence feeding the $19/2^-$ state), which at the same time requires energy differences from the lowest band-members to other states that match several lines left over in the clean spectrum of Fig. 7. Angular correlations indicate that the in-band transitions are stretched quadrupoles and that the 620 keV line is most likely a stretched quadrupole. We do not have good angular correlation values for the 1184 keV transition. However, the spins given in Fig. 6 are favored, because, if the 1184 kev were stretched quadrupole also, the 767 keV line would have to be an E3 or M2. If the 1184 keV transition were unstretched, the spins would be lowered by, at most, one unit. With the given spin assignments the superdeformed states become yrast at spin 45/2, and it is around this spin that the intensities of the superdeformed band and the negative-parity states become comparable. Since we do not observe the other signature partner of the superdeformed band, this suggests that in this band the odd neutron may occupy a unique-parity orbital with low-Ω, thus giving a large splitting.

The discrete superdeformed band reaches an intensity level of 1%--about the limit of detection--at transition energies around 1.3 MeV, but there is evidence for superdeformed shapes in the continuum up to 1.6 MeV. A series of cuts perpendicular to the diagonal in the two-dimensional array $E_\gamma(1)$-$E_\gamma(2)$ is shown in Fig. 8. These spectra are dominated by the 4n and 5n products of the reaction (^{136}Nd and ^{135}Nd). At lower spins (E_γ below 1.2 MeV), continuous ridges 136 keV apart ($\mathcal{J}^{(2)} \approx 59\ \hbar^2 MeV^{-1}$) are seen, which contain more intensity than the observed discrete band. Even the second and third ridges, as marked in fig. 8, are reasonably strong. Above 1.3 MeV, where the discrete

superdeformed band fades out, ridges are still present 144 keV apart ($\mathcal{J}^{(2)} \approx 56$ $\hbar^2 MeV^{-1}$). Thus, there must be many unresolved transitions from states which have about the same moment of inertia as the discrete superdeformed band. From 1.3 MeV up to the highest γ-ray energies where ridges can be seen, their separation does not change appreciably. This is a quite different behavior from the discrete superdeformed band, whose dynamic moment of inertia drops appreciably in a smaller energy range, as will be shown shortly (Fig. 11).

Now with two discrete superdeformed bands known in the light rare earths, we started to search for others. High spin states in ^{134}Nd and ^{136}Nd were populated by the ^{98}Mo(^{40}Ar,4n) and ^{100}Mo(^{40}Ar,4n) reactions, at beam energies of 173 MeV and 176 MeV, respectively. The beam was provided by the 88-Inch Cyclotron of the Lawrence Berkeley Laboratory and in both experiments two enriched molybdenum foils (0.5 mg/cm^2) were used as a target, such that the evaporation residues recoiled into vacuum. In the ^{134}Nd case ~80 million three- and higher-fold events were recorded on tape, and there were ~700 million such events in the ^{136}Nd case. In both experiments, the 4n-channel was the most strongly populated. Again each set of data was initially sorted into a correlation matrix, whereby every triple event was broken into three independent E_γ-E_γ pairs. Again ridges with a spacing indicative of superdeformed bands were observed in both matrices, and by the procedure already described for ^{135}Nd the two new discrete superdeformed bands shown in Fig. 9 were found.[21] Since the single-gated spectra from the two-dimensional matrices were not clean because of other strong lines which accidentally overlapped in energy with the gates, use of the original triple

γ-ray coincidence data was made. For each event, every γ ray was tested against gates centered at the energies of the superdeformed band, and if two γ rays were within these gate limits, the third one was updated in the spectrum. Individual spectra were kept for each gate combination of two in-band γ rays, so as to have the possibility of dropping contaminated combinations later. All these individual spectra were summed in the ^{134}Nd case, and only a few combinations (that are also present in other bands or other nuclei) were rejected in the ^{136}Nd case. As a background, the sum of spectra that were single gated on the same energies of the superdeformed in-band transitions (appropriately normalized), was used. The resulting background-subtracted spectra of the superdeformed bands are shown in Fig. 10. It is clear that the two bands are in ^{134}Nd and in ^{136}Nd, respectively. Gates on low-lying yrast transitions in these nuclei indicate intensities of ~4-5% (of the $2^+ \rightarrow 0^+$) for the average of the lower superdeformed band-members in ^{134}Nd and ~2% for those in ^{136}Nd. We were not able to find the linking transitions between the superdeformed bands and the observed yrast transitions, in contrast to the situation with ^{135}Nd. This is not too surprising, since the superdeformed band in ^{135}Nd decays through several observed pathways at its bottom, each carrying less than a fifth of the intensity of the lowest in-band transitions, and several more unobserved transitions. If in ^{134}Nd and ^{136}Nd the superdeformed bands show the same decay pattern, the many linking transitions will be too weak to be seen in our experiments due to the lower intensities of the bands compared to that in ^{135}Nd. Without the direct links, however, the spin assignments given in Fig. 9 have to be regarded as tentative although they are not likely to be

off by more than two units. Also, angular correlation measurements were not possible for the superdeformed in-band transitions because of their low intensities. But their regular pattern suggests that they form a rotational band and are therefore of stretched electric quadrupole character.

The superdeformed band in ^{135}Nd is fed all the way to the lowest transition; the three even nuclei ^{132}Ce, ^{134,136}Nd have a different feeding pattern with no feeding below spin ~26. The feeding out of the superdeformed band is very sudden in all cases. One might think that the differences in the population of these bands are related to the excitation energy of the band. The fact that the ^{135}Nd band with the largest intensity appears to have the lowest excitation energy at a given spin points in that direction. Whether this is due to the alignment that the odd particle contributes or to a pairing effect (i.e., the superdeformed bands have much less pairing than the ground bands) is not clear, and in any case requires that the limiting transitions be found so that the true excitation energies of the bands in the even nuclei can be determined.

The kinematic moments of inertia, $\mathcal{J}^{(1)}/\hbar^2 = I/\hbar\omega$, for the four bands in the Ce and Nd nuclei are very similar if the spins suggested in Fig. 9 are correct. However, a change of even two units in the spin (certainly within the range of experimental uncertainty) changes these moments by 5-15% (depending on the value of I). On the other hand, the dynamic moments of inertia, $\mathcal{J}^{(2)} \approx 4\ \hbar^2/\Delta E_\gamma$, which are independent of the assigned spins, are indeed rather similar as shown in Fig. 11. For that purpose the moments of inertia were scaled to the one for A=134, assuming an $A^{5/3}$ dependence. The band in ^{134}Nd seems to have the smallest moment of inertia, and the band in

^{132}Ce the largest, but the difference amounts to only about 10%. The large fall-off in the dynamic moments of inertia for all four bands at higher frequencies is a dominant feature in Fig. 11. Since lifetime measurements[14] in ^{132}Ce are consistent with a constant deformation of $\beta \approx 0.5$ up to the top transitions (but in fact are not very sensitive to the deformation at the highest spins), and because of the similarities in $\mathcal{J}^{(2)}$ among all four bands, we assume that they all have a similar (constant) deformation. The decrease of $\mathcal{J}^{(2)}$ may then be explained by the gradual alignment in the superdeformed configuration of high-j orbitals whose contribution to the collective moment of inertia is thereby removed.

Information about the probability of staying in the superdeformed band was obtained from the double-gated spectra made from the original triple-coincidence data. For that purpose, we summed the combinations corresponding to pairs of adjacent transitions and those pairs one apart, two apart and three apart, and compared that spectrum with one gated by coincident pairs separated by four or more transitions in the band. One can calculate the intensity ratio expected for these two spectra knowing the relative intensities of the lines and assuming that the decay proceeds completely through the band. Within the experimental uncertainty (which is estimated to be ~30%) the calculated and measured ratios agree for the superdeformed bands in ^{134}Nd and in ^{136}Nd. We can thus exclude a strong feeding in and out at every state; rather the decay path remains in the discrete superdeformed band once it hits one of its members. In fact we can deduce that the probability for staying in band at each step is greater than ~90% (except for the lowest in-band transition). This is what one might expect with large in-band B(E2)'s

associated with the large deformations and relatively small inter-band transition probabilities due to the significant difference in shape of the lower-lying states in the nucleus, but is the first proof of this behavior.

In both experiments, superdeformed ridges were observed in the two-dimensional matrices from ~0.9 MeV to ~1.5 MeV, the upper limit being caused by statistics. The ridges have greater intensity than that of the corresponding discrete band, and appear continuous, rather than made of discrete points. This suggests that they consist of additional unresolved bands beyond the discrete one. The second ridge, though present, is considerably weaker than the first ridge, in contrast to the situation with the discrete band. This indicates a very different decay pattern, namely a large probability for leaving for another band, either superdeformed also, or more usually a normal one. Still another difference is that the dynamic moment of inertia deduced from the ridge separation drops less over the same transition energy range than that of the resolved transitions. This may be due to a variety of configurations in the unresolved bands so that the admixture of various additional high-j orbitals is possible or that larger deformations are induced.

To sum up, we have found superdeformed bands in ^{134}Nd, ^{135}Nd and ^{136}Nd which are very similar to the previously known band[13] in ^{132}Ce. The abundance of superdeformed bands in the Nd isotopes suggests that the superdeformed minimum is a general feature of nuclei in this region. This may be in contrast to ^{152}Dy, where apparently a strong shell effect causes the minimum at very large deformation to be especially deep in that particular case. In the three Nd nuclei, as also in our study[22] of ^{152}Dy, the ridges

in the two-dimensional arrays appear continuous and have more intensity than can be accounted for by the discrete band. The states in the latter show no decay out of the band until the last couple of transitions, while the continuum bands show the opposite behavior, with little probability of staying in the original band for more than 2 or 3 transitions. A picture consistent with these results is that the discrete band is the "yrast" band for the superdeformed shape and the unresolved bands are higher-lying ones. But this leaves many questions unanswered. How do the bands decay out so rapidly at the bottom? How strong are the pairing correlations in the superdeformed bands? Are there a variety of configurations in the superdeformed bands in the continuum? Why is ^{152}Dy the only example observed so far in the mass 150 region? How strongly are superdeformed states fed in the original population of excited states after neutron emission in a (H.I.,xn) reaction? And many more.

The Damping of Rotational Motion

The possible existence of rotational damping in nuclei at high spin and temperature is a topic that has only come up in the last few years, and I shall describe part of our studies of the past year.

As better instrumentation has enabled spectroscopic studies to push to higher and higher spins in the nucleus, the intensities of the yrast and near-yrast discrete transitions go down and down, to the order of 1% (of the ground-state transition) at spin 40ħ in the rare-earth products of a (^{40}Ar,4n) reaction. Most of the population is in excited states ranging up to 10 MeV, or more, above the yrast line, and there are an enormous number of de-exciting cascades possible. Thus, if we want to know about high-spin states and their

transitions, we have to understand the resulting continuum spectra. Figure 12 shows the total projection of the γ-γ matrix for the decay cascades of ^{159,160}Er. The very strong peaks at low γ-ray energies are the discrete near-yrast transitions, but they become negligible above 1 MeV. Statistics are not a problem in this spectrum; there are hundreds of thousands of counts per channel in the peaks. Under the discrete peaks is the continuum spectrum; this is made of two components. The smaller one is composed of the statistical transitions, mostly stretched and unstretched E1 transitions with a probability distribution roughly like $P(E_\gamma)=NE_\gamma^3\exp(-E_\gamma/T)$. This function is drawn in as the smooth curve in the figure and is normalized to the total intensity in the exponential tail above 2 MeV. The remaining (major) part of the continuum spectrum, the yrast bump, is composed predominantly of stretched E2 transitions. This latter conclusion comes from measurements of the angular distributions and correlations of the γ rays and the few conversion-electron and polarization experiments that have been performed (see, for example, ref. 23 for a review of these experiments). The highest-energy transitions in the yrast bump, those forming the upper edge, move to higher energy with an increase in the angular momentum input to the nucleus. This has been observed by changing the bombarding energy of the projectile, and more clearly by studying the spectra in coincidence with successive slices of the energy in a sum-spectrometer or with successive folds of a γ-ray multiplicity filter.[23] This correlation, that the γ-ray energy is proportional to the spin, and the dominant-stretched E2 character of the transitions strongly suggest that rotational motion is involved. Another type of measurement which shows more directly the collectivity of the cascades is the determination of the average

transition lifetime for a certain range of transition energies. The earliest estimates came from recoil-distance Doppler-shift studies to measure the lifetimes of the lower-spin discrete transitions;[23] the feeding times to the states being measured were also determined and gave upper limits of a few picoseconds for the dozen nuclei studied. Since this feeding involved 10-20 transitions, the individual transition, on the average, took a fraction of a picosecond. With an average γ-ray energy of ~1 MeV this indicated strongly enhanced transitions if taken to be E2. More detailed measurements[24] by DSAM gave average collectivities of 150±50 s.p.u. for the continuum γ rays from about 800-1200 keV for several erbium nuclei from mass 153 to 160. So there are a number of indications that the continuum region at high spin is made up predominantly of rotational cascades.

But for several years it has been recognized that there is a serious problem in considering the continuum γ rays to be members of rotational bands. Consider, the relation between E_γ and spin for a good rotor

$$E_\gamma(I \rightarrow I - 2) = (4I-2)\hbar^2/2\mathcal{J}$$

For a constant moment of inertia, such a spectrum is a series of equally spaced lines as shown in fig. 13 and no two gamma rays have the same energy. Then, in a two-dimensional $E_\gamma(1) - E_\gamma(2)$ array, the diagonal is zero and the pairs of discrete lines form rows of points (ridges) parallel to the diagonal. (The distance between the ridges across the diagonal is $8\hbar^2/\mathcal{J}^{(2)}$, and this is a good way to determine this quantity in the continuum.) Figure 14 shows such a two-dimensional correlation matrix for ^{166}Yb from pairs of Ge detectors. There is indeed a diagonal valley and several ridges can be seen, as well as the horizontal and vertical stripes that come from coincidences with the strongest discrete lines in the spectrum. But the threshold in this

plot was set high to emphasize the valley, and this is one of the better examples of a valley known so far. In fact, the valley is not very deep, becoming even shallower at larger E_γ and disappearing completely above $E_\gamma \approx 1.2$ MeV, as do the ridges. This shallow valley and fading out of the rotational features at higher γ-ray energies was a great disappointment in the initial γ-γ correlation studies of a few years ago. But it indicates clearly that the bands in the continuum are not those of a good rigid rotor. A minimum requirement is that they involve a distribution of transition energies at a given spin. It is not sufficient that there be many bands, each with its own different, but constant, moment of inertia; the individual bands themselves must have the distribution in transition energies in order to fill in the valley.

In the last few years techniques have been developed to measure the width and depth of the valley, and then using simple models one can determine the transition-energy spread.[25-27] First attempts gave values of ~100 keV for this spread. But we were not able to simultaneously fit the width and shallow depth of the valley without postulating an additional wider spread. Two years ago an explanation was made that involved the idea of rotational damping.[28] The idea has two basic ingredients. First, as the excitation energy, E*, above the yrast line (or more accurately, above an energy, U_0 = ~1 MeV, above the yrast line) increases, the level density goes up very rapidly, and at some excitation the levels are so close together that the residual interactions mix them over an interval that itself grows with the excitation energy (as $E^{*3/2}$ in the model of ref. 28). Second, the individual basic rotational bands that mix have different transition energies at the same spin, that is, different moments of inertia. As a result, the decay from a mixed state has a distri-

bution of transition energies, a transition energy spread (not the same as the mixing interval). If it is large enough this spread fills in the valley and smooths out the ridges. But both features are needed; in the absence of the mixing of states, the distribution of moments of inertia would broaden the ridge, but not fill the valley inside a limit given by the largest moment of inertia. And if there is mixing, but only one moment of inertia, then there is no effect on the valley or ridges.

In this model, the transition-energy spread increases at first with excitation energy, and then at still higher excitation decreases. The authors have made estimates of this spread by ascribing the distribution in the moments of inertia of the initial rotational bands to differences in particle alignment. In the rare-earth region around spin 40$\hbar$ they estimate values of ~100 keV, in striking agreement with the two different experiments. However, some very recent calculations[29] indicate that there are also contributions to the transition-energy spread due to shape fluctuations, particularly at higher excitation, that were not included in the earlier calculation. It is not settled yet, but these shape fluctuations might be the origin of a wider energy spread. Finally, we must consider more carefully in what part of the γ-ray cascades damping is most likely to occur, that is, to show its effects. In the cascades following neutron evaporation, the cooling statistical transitions compete best with the rotational transitions when the latter have, on average, small transition energies at lower spin. On average, then, the high-spin, high-energy rotational transitions will have a higher excitation energy above the yrast line than the low-spin, low-energy ones. (This is why we see the discrete lines only at lower spins; at higher spins the population is spread over a much large range of excitation energy.) Thus

from the theory the high-spin transitions should be more highly damped, as the mixing increases with temperature, and the effects of damping should be most visible with the higher-energy transitions, at least up to the point where rotational narrowing sets in.

In the last year we have repeated the γ-γ correlation study on ^{159,160}Er, but using the Ge detectors of HERA, and trying to evaluate the effect on the coincident γ-ray spectrum of requiring a gate having a particular energy and width.[27] There is always one whole transition, the gate, that must be missing from this (coincident) spectrum. In the case of a single, undamped cascade, one sharp transition (the gate) should be missing and the spectrum should drop to zero at the gate position. But with a γ-ray spread, the missing transition is distributed over an energy related to the width of this spread, producing a "dip" in the spectrum, whose depth is inversely proportional to its width. Two gated spectra are shown in Fig. 15; the lighter one is the full projection of the coincidence matrix from (mainly) ^{159}Er and ^{160}Er, and the darker spectrum is coincident with a narrow gate (24 keV width) at 1.1 MeV. The dip, resulting from the narrow gate, is obvious, but its area corresponds to only about 15% of a transition. For gates at higher γ-ray energies the area becomes even smaller, and at energies above 1.3 MeV, the dip disappears completely. (Note that the full coincident spectrum represents 20-25 transitions.) However, it can be reasonably well identified between 0.8 and 1.3 MeV where its width is ~90 keV, and its intensity starts out as ~30% of one transition before dropping to zero with increasing E_γ. The intensity pattern of this dip is very much like that of the resolved lines, which, in this spectrum, also become too weak to be observed somewhere between 1.2 and 1.3 MeV. This is an argument that the dip

like the ridge, is a rather "cold" effect. Cold, undamped bands (each having somewhat different moments of inertia), would give widths around 100 keV, in reasonable accord with the 90 keV observed.

But the fact that this narrow dip is a weak feature (~30% of one transition) already at γ-ray energies around ~0.8 MeV (spins 25-30$\hbar$), and disappears above 1.3 MeV must be reconciled with the loss of one whole transition. A number of explanations may be possible, but it seems to us that the simplest one is that the bulk of the population must have a considerably larger spread in the γ-ray energies so that the corresponding dip is too shallow to observe easily. Only this larger spread would occur above ~1.3 MeV (spin ~50$\hbar$). From the relationship between E_γ (or spin) and temperature, it is likely that this large spread arises from the highest temperature region, and this is most likely to be a damping effect. The width of this broad component is difficult to measure, but limits can be set. It must be considerably greater than 100 keV in order to produce a dip too broad to be observed in Fig. 15. On the other hand, sum-energy gates and multiplicity gates <u>do</u> show correlations of $\bar{E}_\gamma$ with I, which require this width to be less than ~400 keV. Figure 16 illustrates two methods by which we try to measure this width. Figure 16a shows a hypothetical feeding curve, taken to be constant over the upper half of the spin range. This could occur, approximately, if a heavy-ion reaction was used that limited the maximum angular momentum to ~60$\hbar$, and the lower edge was defined by selecting a minimum total γ-ray energy or multiplicity. Since each fed spin decays through all those below itself, such a feeding curve produces a spectrum like the lighter solid line in Fig. 16b. We assume here that all moments of inertia are equal and constant so that E_γ is strictly proportional to spin.

The spectrum in coincidence with a gate in the feeding region, G_H, is illustrated by the heavy solid line in Fig. 16b (the dip associated with the gate width is ignored). Only spins above the γ-ray energy of G_H can contribute to the spectrum, so that, with our assumptions, it will not continue to rise below G_H. If it does so, then E_γ is not strictly proportional to spin, and we assume that in this region of E_γ (1.0-1.5 MeV; 40-60$\hbar$) the main cause is a spread in the γ-ray energies emitted by each rotational state. Then the energy range below G_H over which the spectrum continues to rise is a rough measure of the width of this spread in energies. Figure 17 shows such a spectrum with the gate energy G_H = 1.4 MeV indicated. One must average the discrete lines into the spectrum to draw the horizontal line, but however roughly that line is drawn, the intersection gives a value of about 350 keV below the gate, from which we estimate that the FWHM of the γ-ray spread from each rotational state is around 250 keV. (The main difference between these numbers comes because the spread is involved twice.) Between 1.0 and 1.5 MeV, there seems to be an increase in this spread from ~160 to 280 keV, but this is not very clear.

A different way to evaluate the width involves a second lower gate,[27] G_L, from which we estimate the FWHM of the spread to be 180 keV at 1.22 MeV, reasonably consistent with the above estimates. Neither of these methods is very reliable, and the interpretation depends on feeding patterns and moment-of-inertia variations which we do not know, so we estimate overall uncertainties at 30-40%. If we associate this broad component with a transition-energy spread, then the present indications are that between 40 and 60$\hbar$ it is in the range 150-300 keV, probably increasing with E_γ(spin). We have also performed two more types of studies[30,31] trying to learn more about

where the rotational damping occurs and the magnitude of the damping width. I shall describe only the most recent one[31] because of time limitations and because it can only be done with an array of detectors. We have examined the correlations among three γ-ray energies at high resolution and compared them with the correlations among two γ-ray energies. The first result seems to be a rather clear indication that the main damping widths are indeed large compared to 100 keV.

We studied the reactions, ^{48}Ti(215 MeV) + ^{124}Sn → ^{168}Hf +, ^{40}Ar(180 MeV) + ^{124}Sn → ^{160}Er +, and ^{40}Ar(176 MeV) + ^{100}Mo → ^{136}Nd +, using beams from the LBL 88-Inch Cyclotron. In each case the main (4n) product is given, but there are a couple of others (indicated by the "+") made in sizable yield. The data were taken on HERA, and between 3 and 7 x 10^8 three- and higher-fold events were taken in each of the three cases. These were sorted into symmetrized 250-channel three-dimensional matrices beginning at 200 keV with 8 keV per channel. These were unfolded to correct for the response function of the germanium detectors and, in addition, statistical γ rays, which are essentially uncorrelated, were subtracted using a spectral shape, E_γ^3 exp $(-E_\gamma/T)$, normalized to the high-energy part of each spectrum. Thus single- and double-gated spectra from these matrices should not be influenced by either detector response or statistical γ-rays.

Single-gated spectra were generated by taking the full projection of the two-dimensional matrix (plane) in coincidence with a single (8 keV) channel of the third dimension. A number of full projections of consecutive planes were added, but only after shifting their individual energy scales so that the gates were aligned. Thus, features correlated with the gate were preserved

with no loss of resolution, whereas those not correlated with the gate were smeared out. To generate the double-gated spectra, a second gate was made at the same energy as the first gate. Again a number of spectra from neighboring gates were shifted to align the gates, and added in order to obtain better statistics. The double-gated spectra had effectively one 8 keV gate and one 24 keV gate; the wider 24 keV gate gave a factor of three better statistics and essentially no additional smearing detectable with our statistics. The single- and double-gated spectra were normalized to the same number of counts (The double-gated spectra with two transitions missing rather than one should perhaps better be normalized to 4-5% fewer counts, i.e., to a total multiplicity one less than the single-gated spectra.), and are shown superposed in Fig. 18 for the three reaction systems. It can be seen that there is very little difference between the single- and double-gated spectra. What does this mean? To understand what the damping will do to such spectra, we have developed a computer code to simulate the cascade. In the code an initial spin and excitation energy are chosen at random from reasonable distributions. Then a cascade of rotational- and statistical-type transitions de-excites the nucleus. At each step of this cascade, the transition type is chosen at random from the two possibilities, weighted by the expected transition probabilities. The rotational properties are the most important parameters, and at low temperature, good rotational bands are taken whose properties (moments of inertia and alignment) are chosen (initially, and following each statistical transition) at random from reasonable distributions. Above some critical temperature, where the damping is supposed to set in, this type of rotational behavior ends and every rotational transition energy is chosen at random from a gaussian distribution whose FWHM

("damping width" or Γ_{rot}) is a particular chosen value. It is essential to realize that at low temperatures band properties are chosen at random, but then the cascade typically stays in that band for several transitions (producing the E_γ-E_γ correlations), whereas at high temperatures every rotational transition energy is chosen at random within an energy range determined by Γ_{rot}.

Since the dips in Fig. 17 all have a FWHM around 100 keV, a first trial in the simulation is simply Γ_{rot} = 100 kev for all temperatures. The average moment of inertia is taken to be 60 MeV^{-1}, and the gates are always 8 keV wide and placed at 1.2 MeV. Fig. 19a shows the result of this calculation, which can be easily understood. Both dips have roughly the FWHM of Γ_{rot}, and areas of one and two transitions, respectively, for the single- and double-gated spectra. This does not match experiment. One can make the calculation somewhat more realistic by having good rotational behavior below an excitation energy of 2 MeV above the yrast line (T=0.3 MeV), and damped behavior above that, with Γ_{rot} still equal to 100 keV, as shown in Fig. 19b. Some features are better here (e.g., the ridge structures beside the dip due to the low-temperature undamped bands, and the steeper side walls of the dip due to the innermost ridges whose separation is determined by the moment of inertia), but the factor of two difference in area between the single- and double-gated spectra is unchanged, as is the large dip area, in striking disagreement with the data. Since there must be one and two transitions missing in the single- and double-gated spectra, respectively, the simplest solution we have found is to make the main damping width large, so that the associated dip becomes quite wide and therefore difficult to see. Changing Γ_{rot} from 100 to 300 keV gives the spectra in Fig. 19c, which now begin to look very much like the data, both

in the absolute and relative areas of the dips. The broad dip corresponding to the 300 keV Γ_{rot} can hardly be seen in these spectra, and the apparent dips come from the undamped cascades below T=0.3 MeV. To understand the similarity in the single- and double-gated spectra, one should remember that one gate on an undamped γ ray removes all undamped γ rays of that energy (the dip in undamped cascades goes all the way to zero). Thus, the second gating γ ray must come from the broad damped distribution, which does not affect the narrow dip very much. These data, and other experiments not described, suggest the overall picture; an observed dip that is (nearly) undamped from states at low excitation, together with a broad (~300 keV), so unobserved, damping width at higher temperatures. However, this analysis represents only the first step in extracting information from three- and higher-fold data; we feel that in the future they hold great promise for giving us a much more detailed understanding of the damping process.

While the general behavior of these "warm" rotational bands is becoming clearer, there remain many open questions. For example, we would like to know the excitation energy or temperature at which the damping sets in, as this is the point where the average separation between levels of a given spin becomes comparable to the average matrix element connecting these levels. How suddenly does the damping set in? Since we see only essentially undamped and strongly damped behavior, a rather sudden onset of the damping is indicated (as is expected by theory), but more specific information would be interesting. How complete is the damping, i.e., are there types of states (like superdeformed or strongly triaxial ones) that have much smaller matrix elements connecting them with the bulk of the states, and therefore remain largely undamped over our populated temperature regions? In this connection,

Egido[29] found that alignment variations may be damped before the normal shape variations. Finally, it would be nice to have more direct evidence that damping is indeed the process causing the observed effects. For example, the onset of large irregularities in the rotational-band energies above 2 MeV due to more triaxial shapes could explain the dip behavior, and although it is considered less likely for a number of reasons, it is not completely ruled out. There is so much to do.

I hope these two examples of studies have shown you the power of the new detector arrays, and illustrated how little we know and how much there is to learn. Hopefully, some of these questions will be answered at the next Zakopane Workshop.

Acknowledgments

The work on superdeformed bands in the Nd isotopes was principally analyzed by E.M. Beck, and that on rotational damping by F.S. Stephens. But all the members of the group contributed during the past year: J.C. Bacelar, M.A. Deleplanque, J.E. Draper, C. Duyar, J.L. Egido, R.J. McDonald, and A.O. Macchiavelli. In addition, I would like to thank M. Lee and R. Belshe for their critical help with the electronics and computer software, respectively.

References

1. R.M. Diamond and F.S. Stephens, "The High Resolution Ball" (proposal, unpublished, 1981); R.M. Diamond, "The Berkeley High Resolution Ball," Instrumentation for Heavy-ion Research, p. 259 (Harwood Academic Pub., New York, 1985).

2. S.M. Polikanov, V.A. Druin, V.A. Karnaukhov, V.L. Mikheev, A.A. Pleve, N.K. Skobelev, V.G. Subbotin, G.M. Ter-Akop'yan, and V.A. Fomichev, Soviet Physics JETP 15, 1016 (1962).

3. A. Bohr and B.R. Mottelson, Nuclear Structure, Vol. II, p. 622 (W.A. Benjamin, Inc. Reading, MA., 1975).

4. K. Neergaard and V. Pashkevich, Phys. Lett. 59B, 218 (1975).

5. K. Neergaard, V. Pashkevich, and S. Frauendorf, Nucl. Phys. A262, 61 (1976).

6. I. Ragnarsson, T. Bengtsson, G. Leander, and S. Aberg, Nucl. Phys. A347, 287 (1980).

7. J. Dudek, A. Majhofer, W. Nazarewicz, and Z. Szymanski, Phys. Lett. 112B, 1 (1982).

8. S. Aberg, Phys. Scr. 25, 23 (1982).

9. K. Neergaard, H. Toki, M. Ploszajczak, and A. Faessler, Nucl. Phys. A287, 48 (1972).

10. T. Bengtsson, M.E. Faber, G. Leander, P. Möller, M. Ploszajczak, I. Ragnarsson, and S. Aberg, Phys. Scr. 24, 200 (1981).

11. C.G. Andersson, R. Bengtsson, T. Bengtsson, J. Krumlinde, G. Leander, K. Neergaard, P. Olanders, J.A. Pinston, I. Ragnarsson, Z. Szymanski, and S. Aberg, Phys. Scr. 24, 26 (1981).

12. J. Dudek and W. Nazarewicz, Phys. Rev. C31, 298 (1985).

13. P.J. Nolan, A. Kirwan, D.J.G. Love, A.H. Nelson, D.J. Unwin, and P.J. Twin, J. Phys. G: Nucl. Phys. 11, L17 (1985).

14. A.J. Kirwan, G.C. Ball, P.J. Bishop, M.J. Godfrey, P.J. Nolan, P.J. Thornley, D.J.G. Love, and A.H. Nelson, Phys. Rev. Lett. 58, 467 (1987).

15. S. Cohen, F. Plasil, and W.J. Swiatecki, Ann. Phys. 82, 557 (1974).

16. P.J. Twin, B.M. Nyako, A.H. Nelson, J. Simpson, M.A. Bentley, H.W. Cranmer-Gordon, F.D. Forsyth, D. Howe, A.R. Mokhtar, J.D. Morrison, J.F. Sharpey-Schafer, and G. Sletten, Phys. Rev. Lett. 57, 811 (1986).

17. E.M. Beck, F.S. Stephens, J.C. Bacelar, M.A. Deleplanque, R.M. Diamond, J.E. Draper, C. Duyar, and R.J. McDonald, Phys. Rev. Lett, to be published.

18. J. Gizon, A. Gizon, M.R. Maier, R.M. Diamond, and F.S. Stephens, Nucl. Phys. A222, 557 (1974).

19. D. Fossan, private communication (1986).

20. O. Andersen, J.D. Garrett, G.B. Hagemann, B. Herskind, D.L. Hillis, and L.L. Riedinger, Phys. Rev. Lett. 43, 687 (1979).

21. E.M. Beck, R.J. McDonald, A.O. Macchiavelli, J.C. Bacelar, M.A. Deleplanque, R.M. Diamond, J.E. Draper, and F.S. Stephens, to be published.

22. M.J.A. de Voigt, J.C. Bacelar, E.M. Beck, M.A. Deleplanque, R.M. Diamond, J.E. Draper, H.J. Riezebos, and F.S. Stephens, to be published.

23. R.M. Diamond and F.S. STephens, Ann. Rev. Nucl. Part. Sci. 30, 85 (1980).

24. H. Hübel, R.M. Diamond, P. Aguer, C. Ellegaard, D.B. Fossan, H. Kluge, C. Schück, S. Shih, F.S. Stephens, and U. Smilanski, Z. Phys. A304, 2251 (1982).

25. F.S. Stephens, Proceedings of the Second International Conference on Nucleus-Nucleus Collisions (North-Holland Pub., Amsterdam, 1985); J.E. Draper, E.L. Dines, M.A. Deleplanque, R.M. Diamond, and F.S. Stephens, Phys. Rev. Lett. 56, 309 (1986).

26. J.C. Bacelar, G.B. Hagemann, B. Herskind, B. Lauritzen, A. Holm, J.C. Lisle, and P.O. Tjøm, Phys. Rev. Lett 55, 1858 (1985).

27. F.S. Stephens, J.E. Draper, J.L. Egido, J.C. Bacelar, E.M. Beck, M.A. Deleplanque, and R.M. Diamond, Phys. Rev. Lett. 57, 2912 (1986).

28. Th. Døssing, Niels Bohr Centennial Conference on Nuclear Structure (Elsevier Science Pub., 1985); B. Lauritzen, R.A. Broglia, and Th. Døssing, Nucl. Phys. A457, 61 (1986)..

29. J.L. Egido, private communication, 1986.

30. F.S. Stephens, J.E. Draper, J.C. Bacelar, E.M. Beck, M.A. Deleplanque, and R.M. Diamond, to be published.

31. F.S. Stephens, J.C. Bacelar, E.M. Beck, M.A. Deleplanque, and R.M. Diamond, Phys. Rev. Lett., to be published.

Figure Captions

1. Outline of cylindrical BGO Compton-suppression shield showing 5x5 cm Ge detector inside, two of six photomultiplier tubes on back surface, and NaI nose cone.
2. Spectra of ^{60}Co taken with bare 20% Ge detector and with Compton-suppressed one (BGO shield and NaI cap). Peaks go 12 times the figure height.
3. Perspective view of one-half the system.
4. Photograph of 12 Compton-suppressed Ge modules (without NaI caps) in place around the target chamber, looking in the direction of the beam pipe.
5. Photograph of 15 modules (with NaI caps) from the side (beam tube goes off to the left); six more modules are pulled back toward camera to allow access.
6. Level scheme of ^{135}Nd, including superdeformed band. Transition energies are given in keV.
7. Double-gated, background-substracted spectrum of lines coincident with superdeformed transitions in ^{135}Nd. Transitions from less deformed states are marked by # symbols; the linking transitions between the superdeformed and less-deformed bands are marked by 1's.
8. Projections perpendicular to the diagonal in the $E_\gamma(1)$-$E_\gamma(2)$ matrix that has had uncorrelated events removed by the method of ref. 20. The top cut is from 1.0-1.2 MeV, the middle is from 1.2-1.4 MeV, the bottom is from 1.4-1.6 MeV. Scale is 4 keV/channel.
9. Superdeformed bands and some yrast transitions in ^{132}Ce, ^{134}Nd, ^{135}Nd, and ^{136}Nd. The dashed arrows indicate unobserved linking transitions. Energies are given in keV, and the data for ^{132}Ce is from ref. 14.

10. Superdeformed bands in ^{134}Nd (top) and ^{136}Nd (bottom) labeled by transition energies. The less-deformed yrast transitions populated by them are labeled by the spin of the initial state. The background-subtracted spectra are a sum of double-gated combinations.
11. Dynamic moments of inertia of superdeformed bands scaled to A=134 by $A^{5/3}$. Open (filled) squares represent ^{134}Nd(^{136}Nd), and open (filled) circles represent ^{132}Ce(^{135}Nd).
12. Total projection of γ-γ coincidence matrix for ^{159,160}Er. Smooth curve is estimate of statistical γ-ray spectrum from $P(E_\gamma) \propto E_\gamma^3 \exp(-E_\gamma/T)$, normalized to high-energy exponential tail.
13. A schematic rotational band, and the resulting γ-ray spectrum from an initial state of spin I_{max}.
14. Plot of $E_\gamma(1)$ vs. $E_\gamma(2)$ for ^{166}Yb coincidences after subtracting uncorrelated components. The diagonal valley and three pairs of ridges can be seen, as well as "stripes" from coincidences with the strongest discrete transitions.
15. Coincidence Ge spectra from ^{124}Sn(^{40}Ar,xn)^{159,160}Er. The lighter line is the full projection of all coincidences, whereas the darker one is coincident with the narrow gate indicated. The initial two-dimensional matrix had been unfolded first.
16. Schematic illustration of a) a plausible feeding curve following a heavy-ion fusion reaction, b) the spectra coincident with gates G_H (heavy line) and G_L (double line), and c) the difference of the two gated spectra.

17. The Ge spectrum projected from the indicated gate; the matrix is that of Fig. 15 but with the statistical transitions removed. the lines (to guide the eye) indicate the two regions of the spectrum (see text).

18. Gamma-ray spectra in coincidence with a single gate (circles) and a double gate (solid line), for a) ^{168}Hf; b) ^{160}Er, and c) ^{136}Nd. The energy regions covered by the (shifted) gates (see text) are: a) 0.68-1.00 MeV; b) 0.60-1.00 MeV; and c) 0.92-1.16 MeV, and they are shifted to center at: a) 0.72 MeV; b) 0.64 MeV; and c) 0.96 MeV.

19. Similar to Fig. 18 but for simulated data with gates at 1.2 MeV: a) fully damped, Γ_{rot} of 100 keV; b) undamped below 2 MeV of excitation on the yrast line, Γ_{rot} of 100 keV; c) undamped below 2 MeV on the yrast line, Γ_{rot} of 300 keV. (The discrete lines are suppressed.)

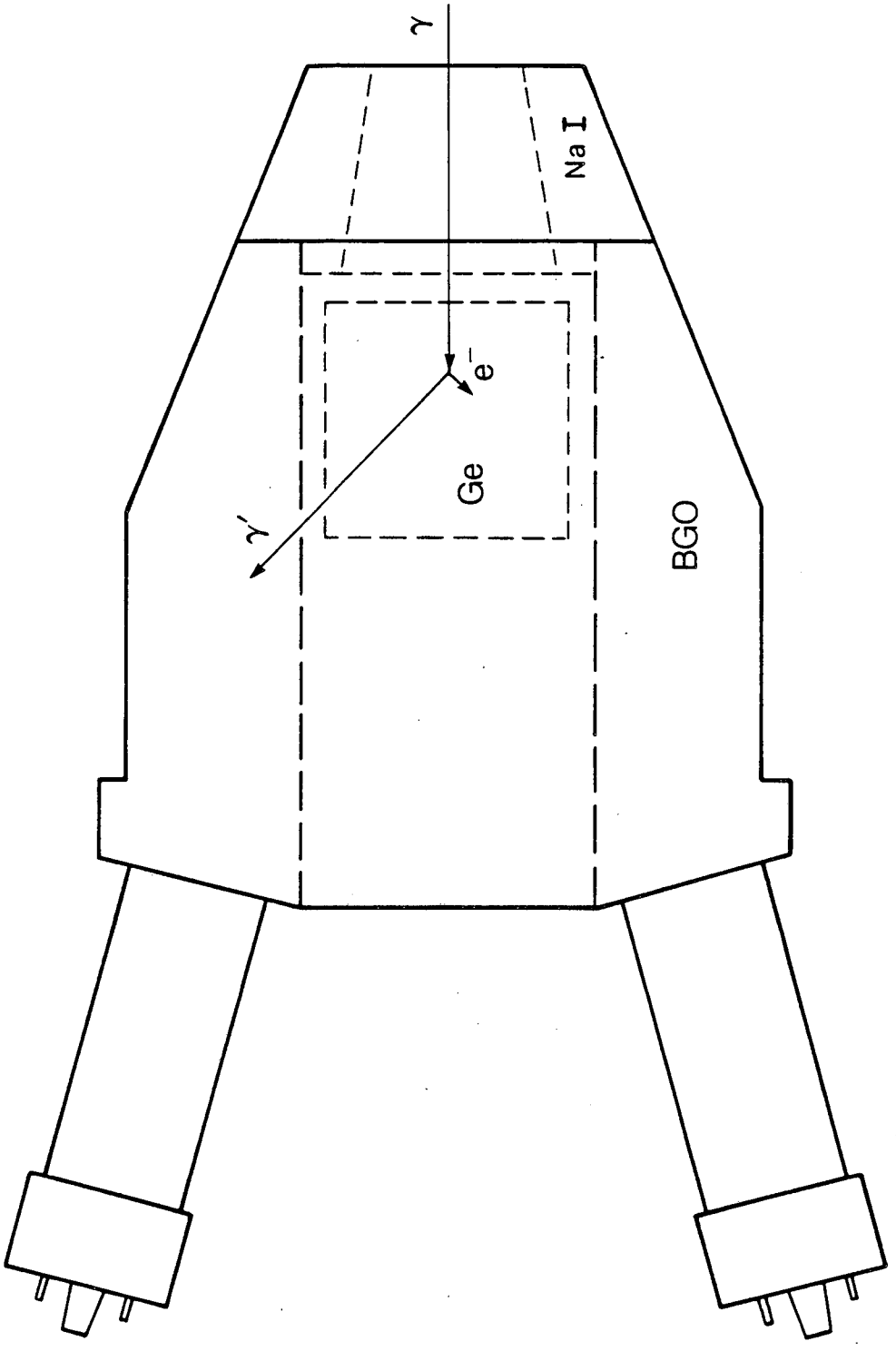

XBL 8411-4840

Figure 1

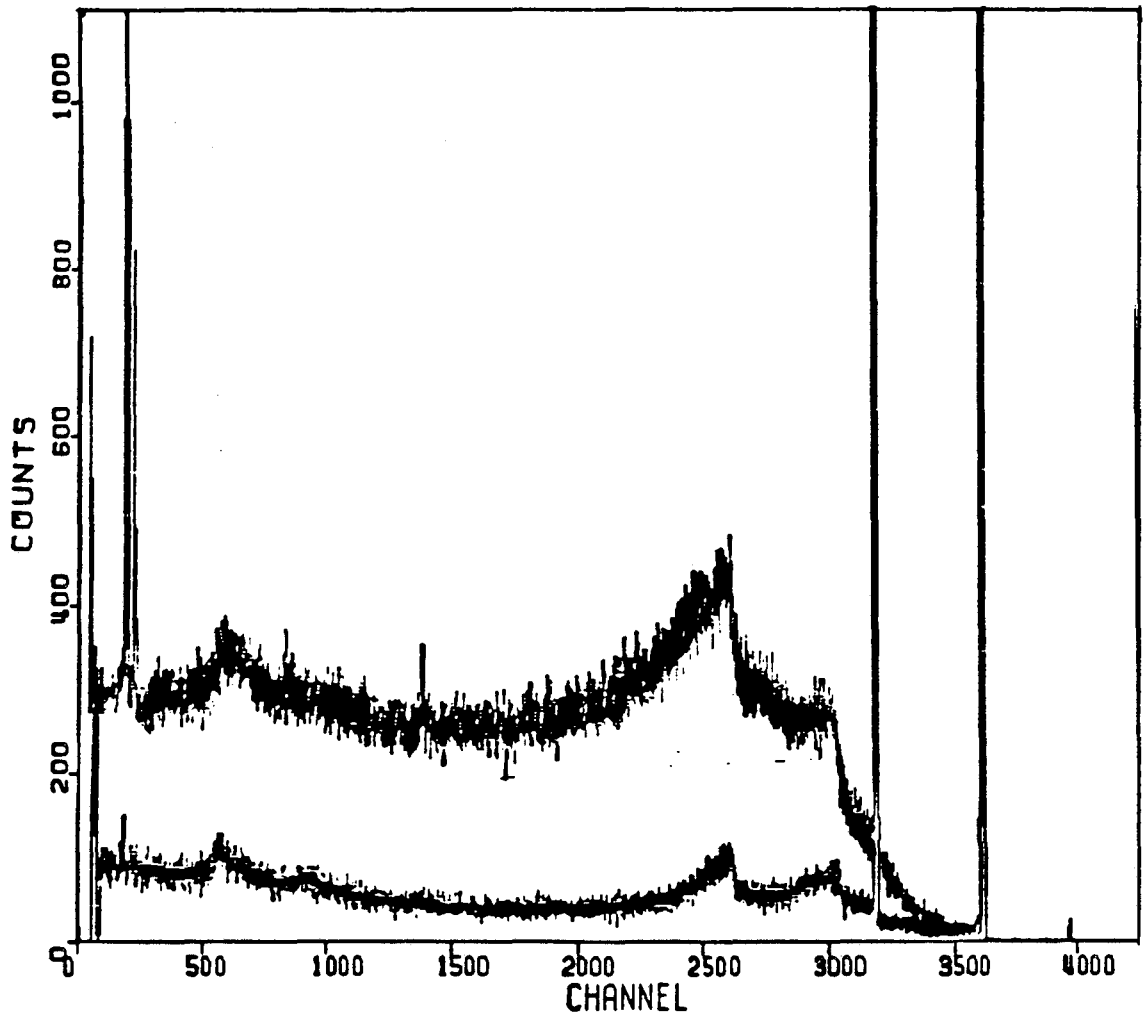

XBL 867-2688

Figure 2

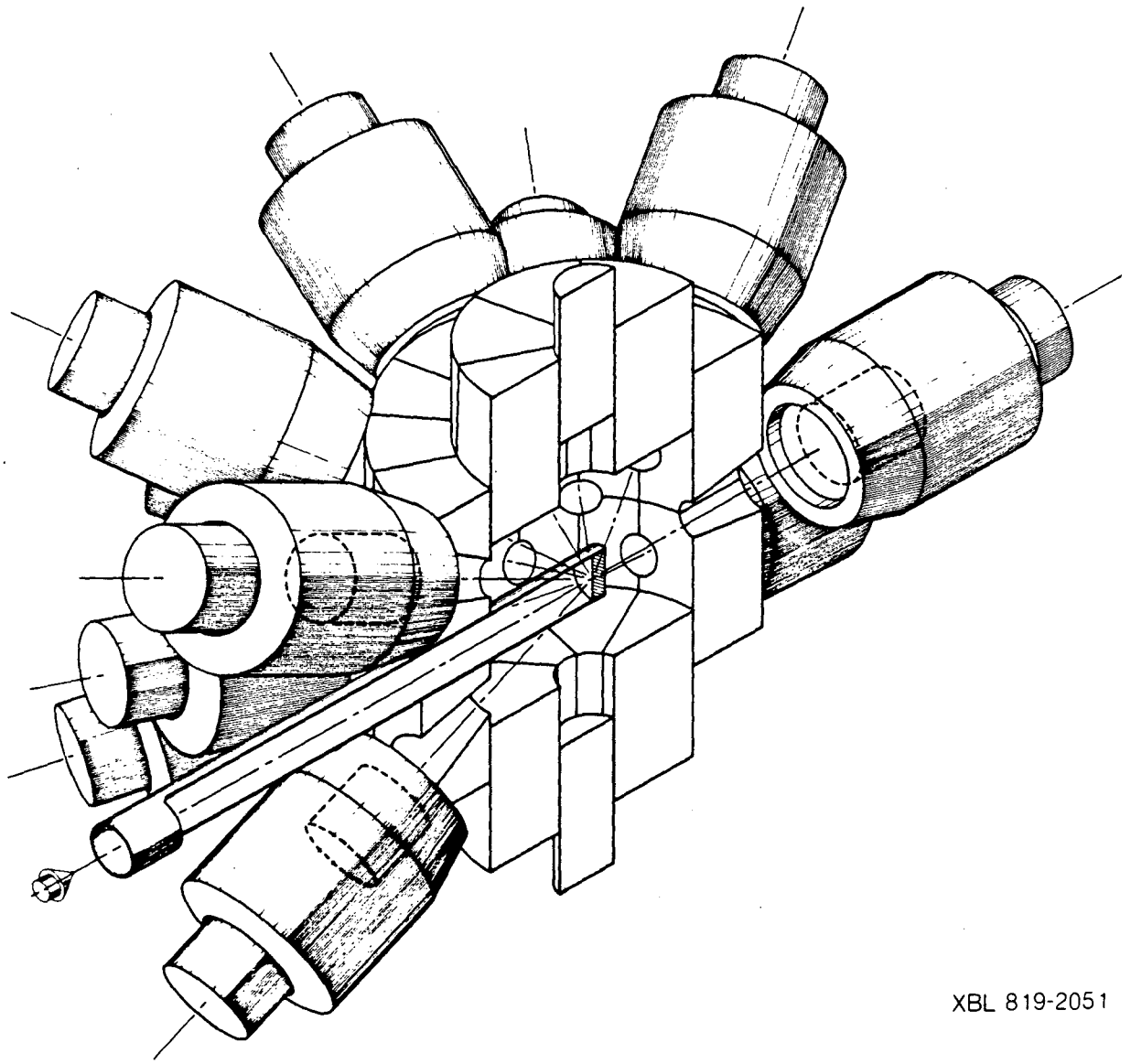

XBL 819-2051

Figure 3

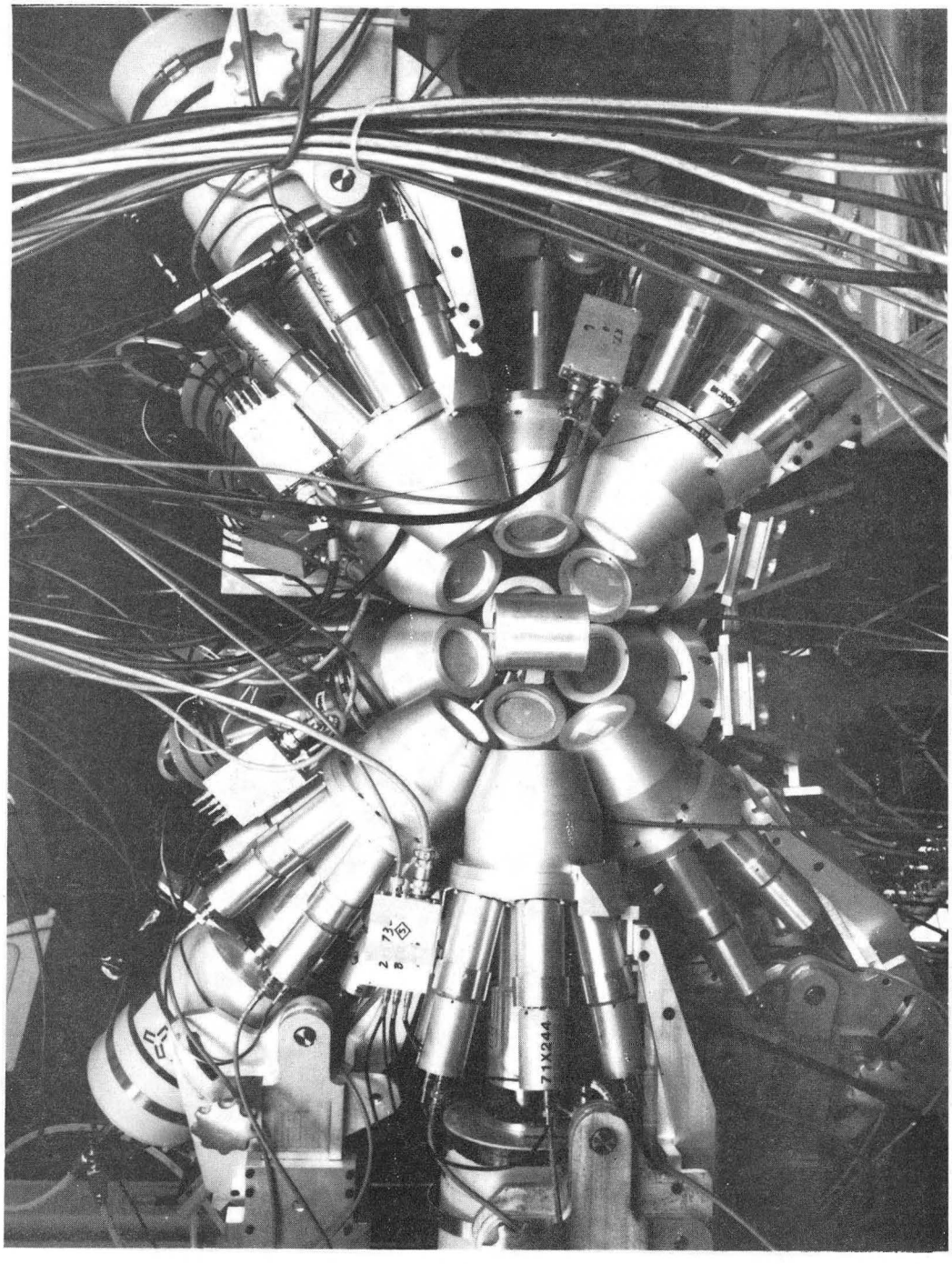

CBB 846-4584

Figure 4

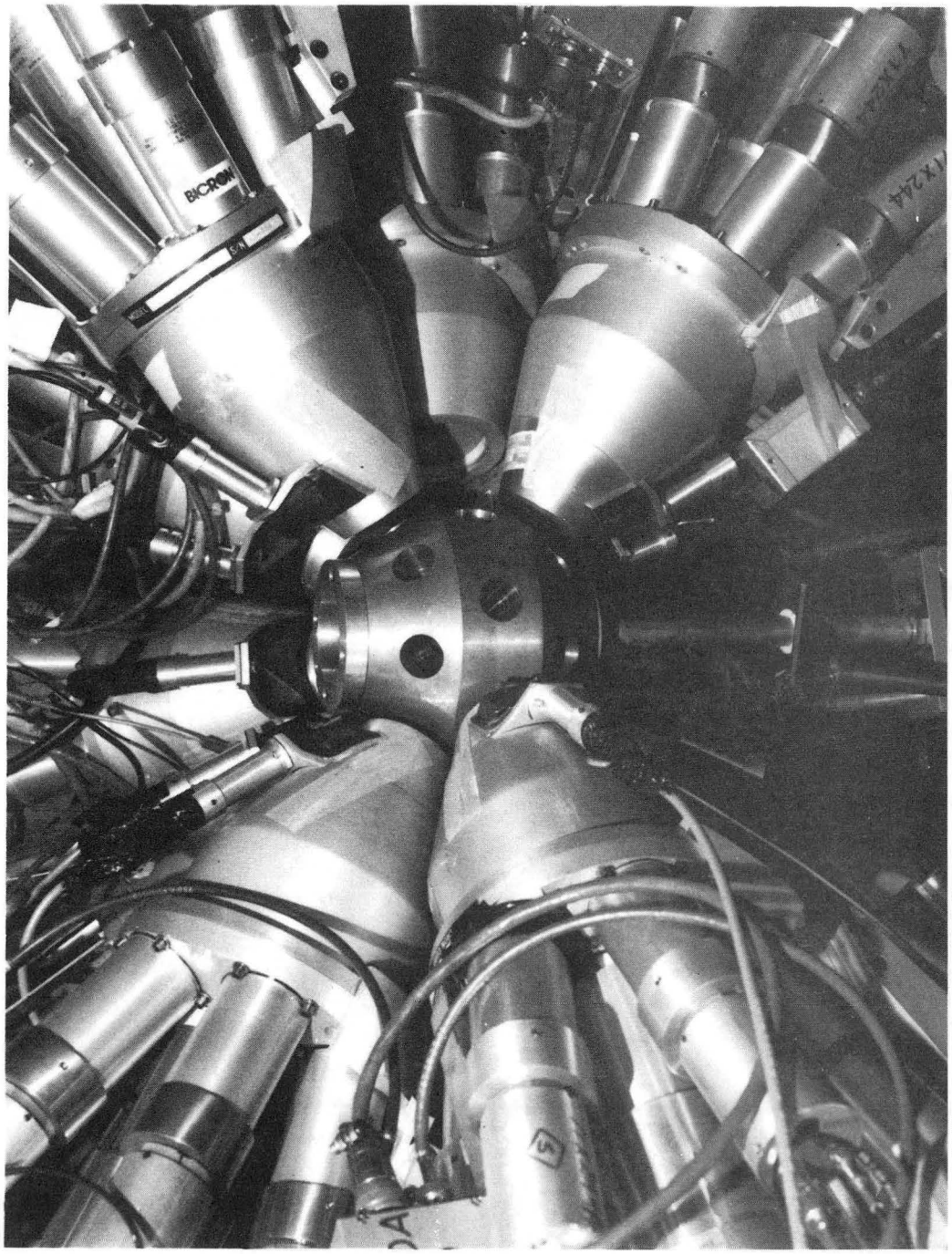

CBB 869-7653

Figure 5

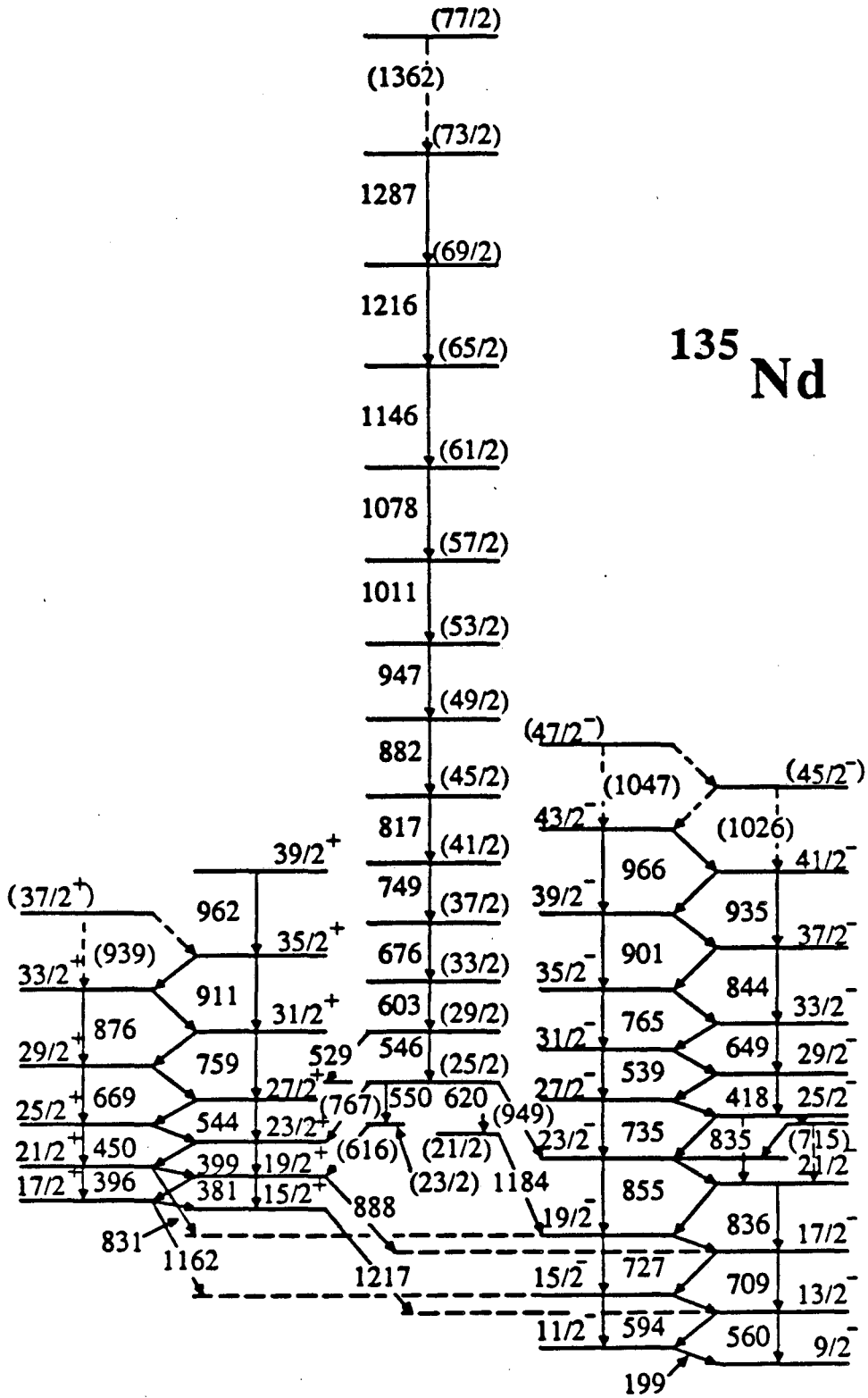
135 Nd
(77/2)
(1362)
(73/2)
1287
(69/2)
1216
(65/2)
1146
(61/2)
1078
(57/2)
1011
(53/2)
947
(49/2)
882
(45/2)
817
(41/2)
749
(37/2)
676
(33/2)
603
(29/2)
546
(25/2)
529
550
620
(767)
(949)
(616)
(21/2)
(23/2)
1184
888
1217
831
1162
39/2+
(37/2+)
962
35/2+
(939)
33/2+
911
31/2+
876
29/2+
759
27/2+
669
25/2+
544
23/2+
450
21/2+
399
19/2+
396
17/2+
381
15/2+
(47/2-)
(1047)
(45/2-)
43/2-
(1026)
966
41/2-
39/2-
935
37/2-
901
35/2-
844
33/2-
765
31/2-
649
29/2-
539
27/2-
418
25/2-
735
23/2-
835
(715)
21/2
855
19/2-
836
17/2-
727
15/2-
709
13/2-
594
11/2-
560
9/2-
199

Figure 6

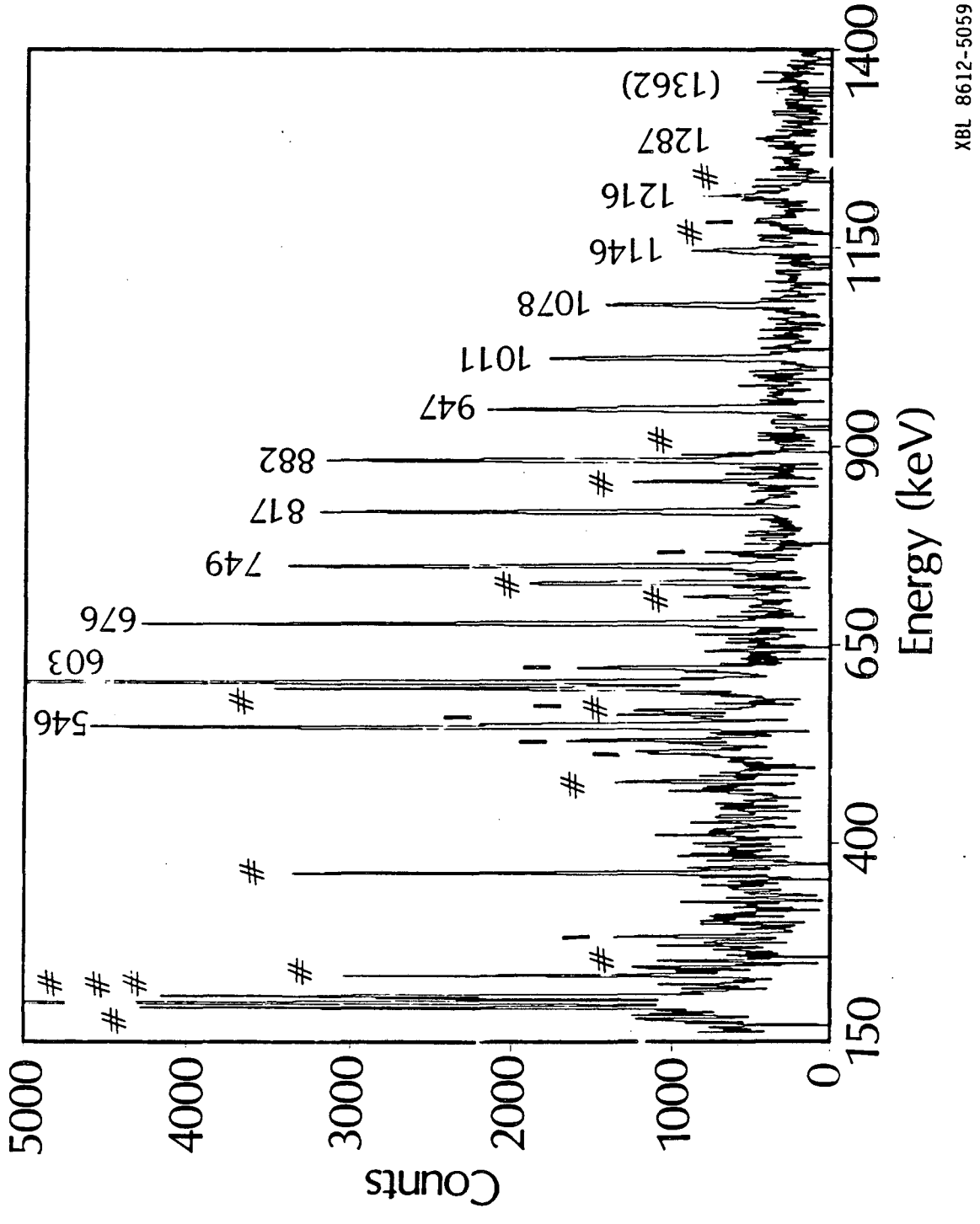
Counts
5000
4000
3000
2000
1000
0
150
400
650
900
1150
1400
Energy (keV)
546
603
676
749
817
882
947
1011
1078
1146
1216
1287
(1362)
XBL 8612-5059

Figure 7

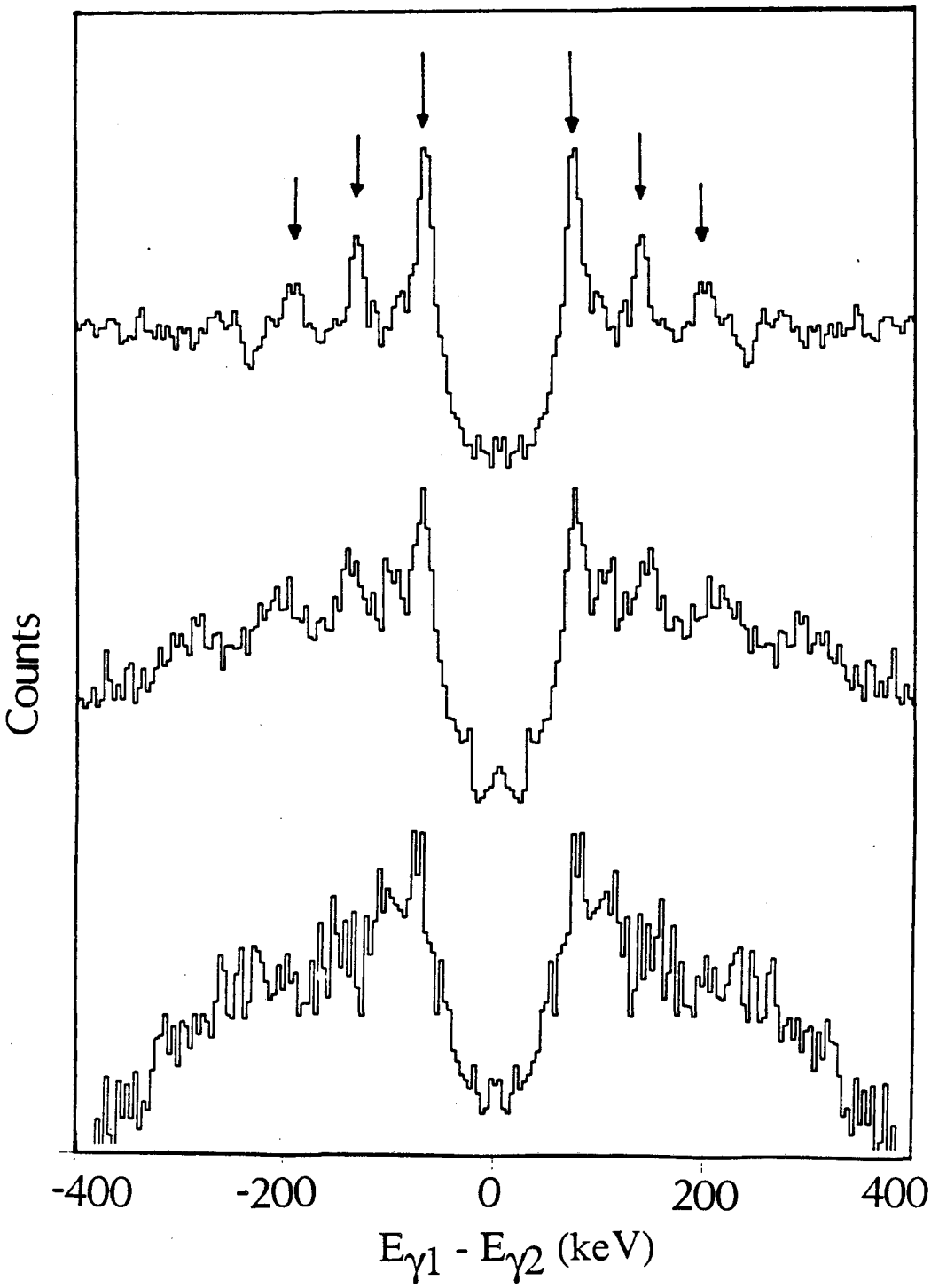

XBL 8612-5061

Figure 8

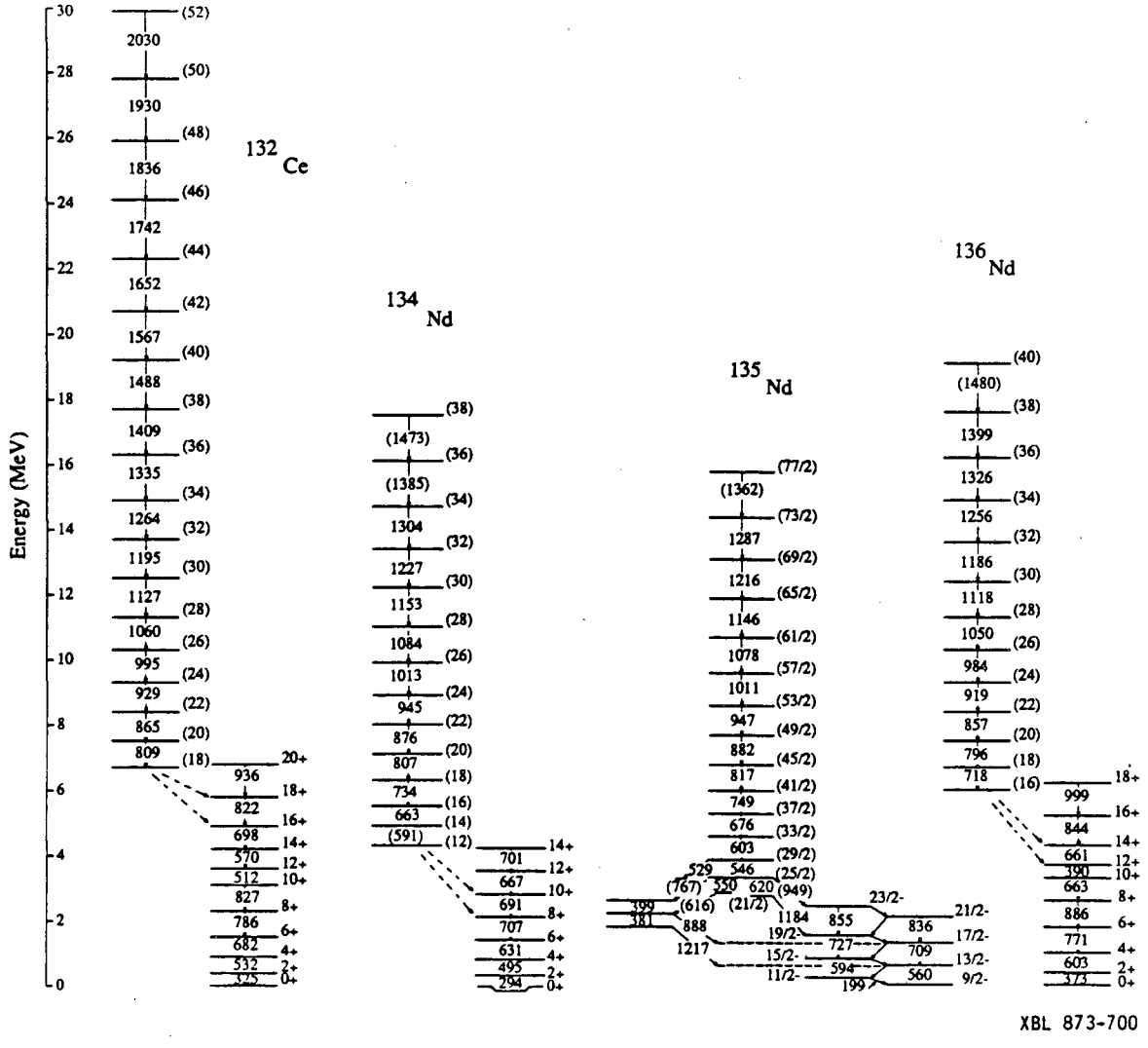

Figure 9

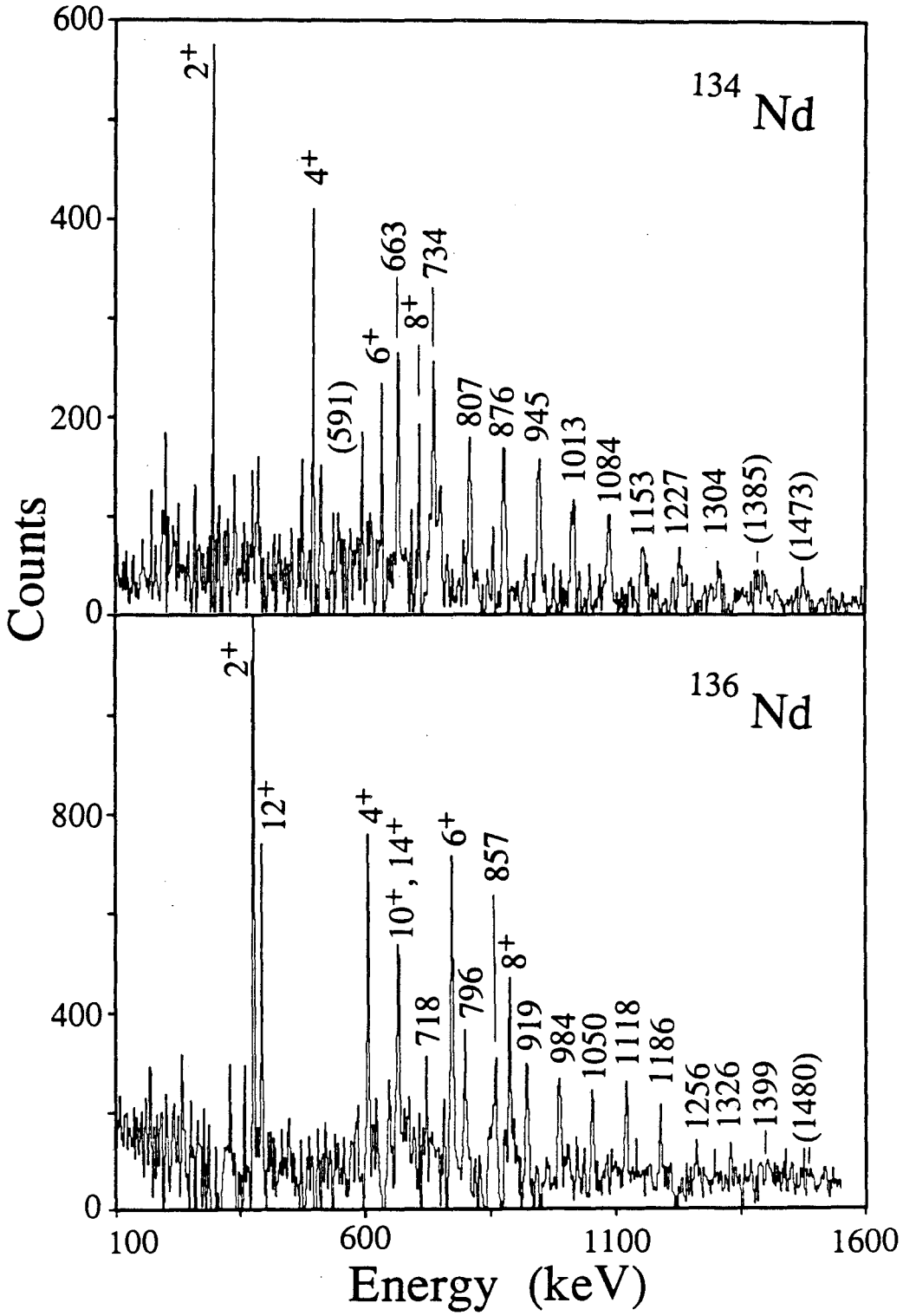

XBL 873-703

Figure 10

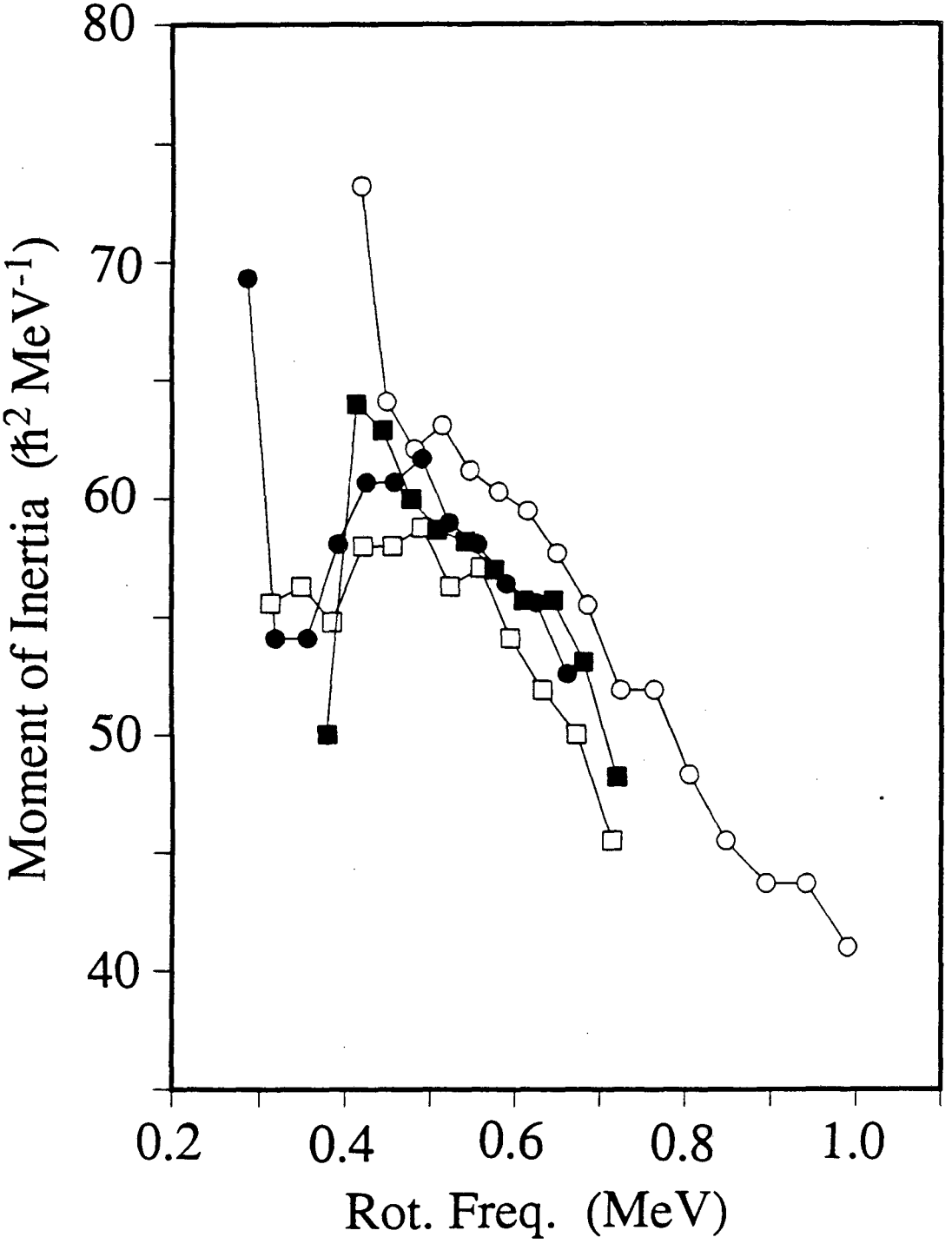

XBL 873-701

Figure 11

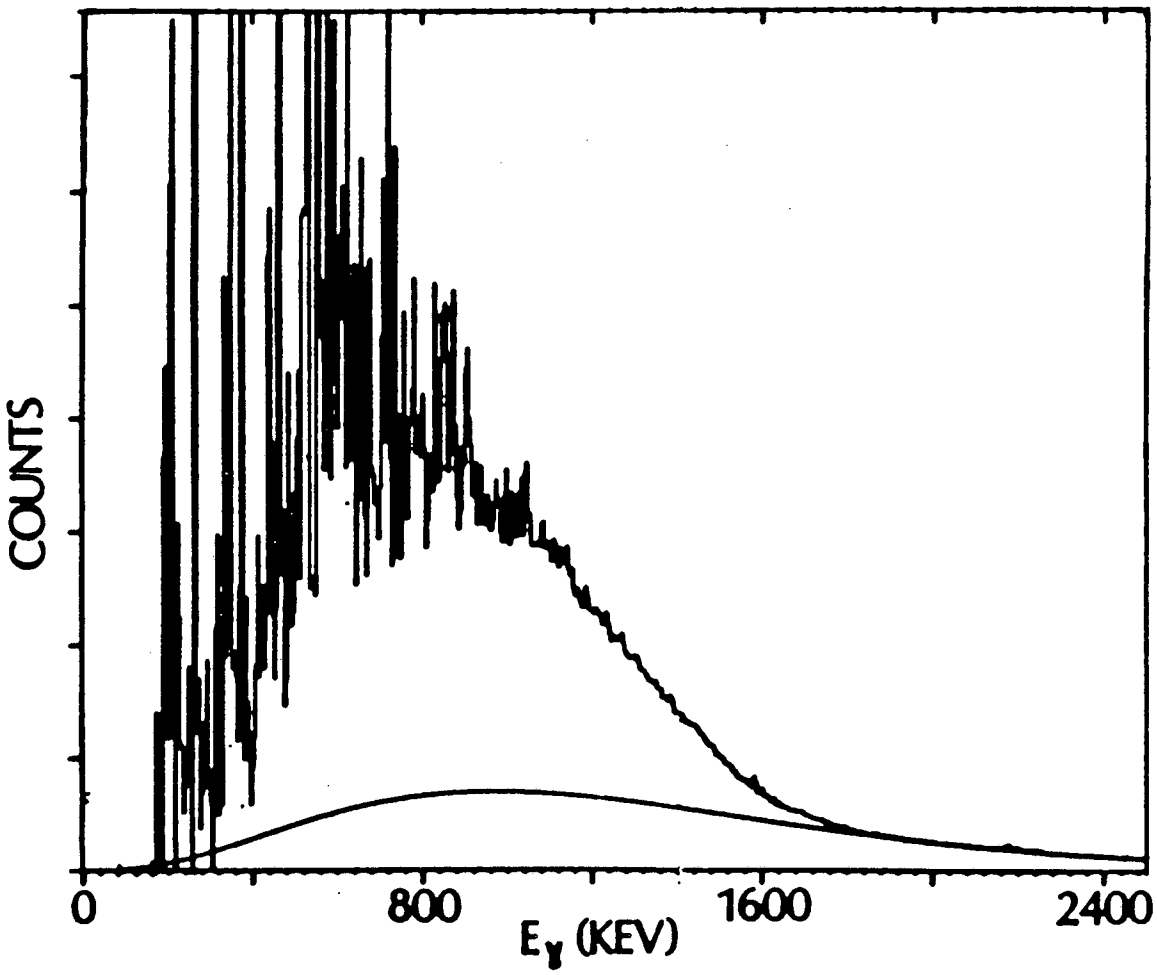

XBL 876 2502

Figure 12

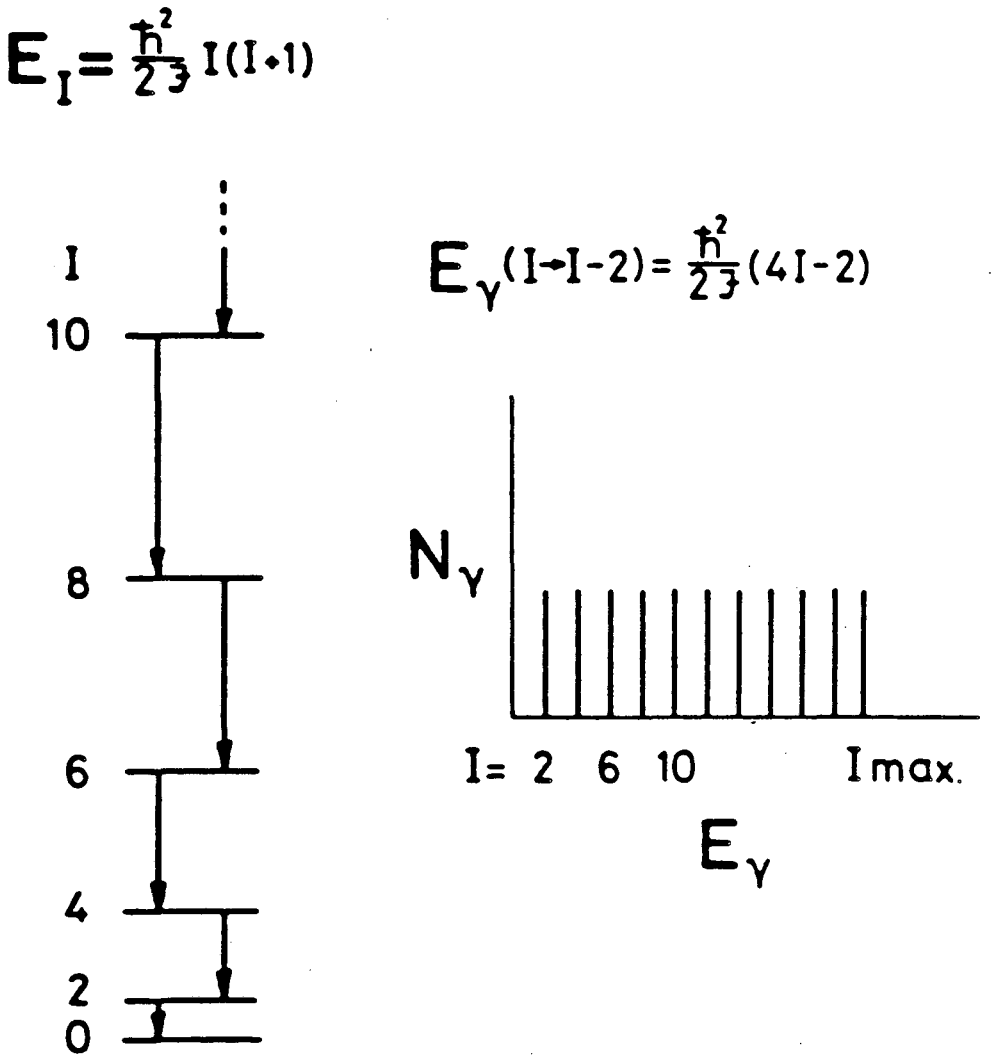
$E_I = \frac{\hbar^2}{2\mathfrak{I}} I(I+1)$
I
10
8
6
4
2
0
$E_\gamma(I \to I-2) = \frac{\hbar^2}{2\mathfrak{I}}(4I-2)$
N_γ
I= 2 6 10 Imax.
E_γ
XBL 867-2684

Figure 13

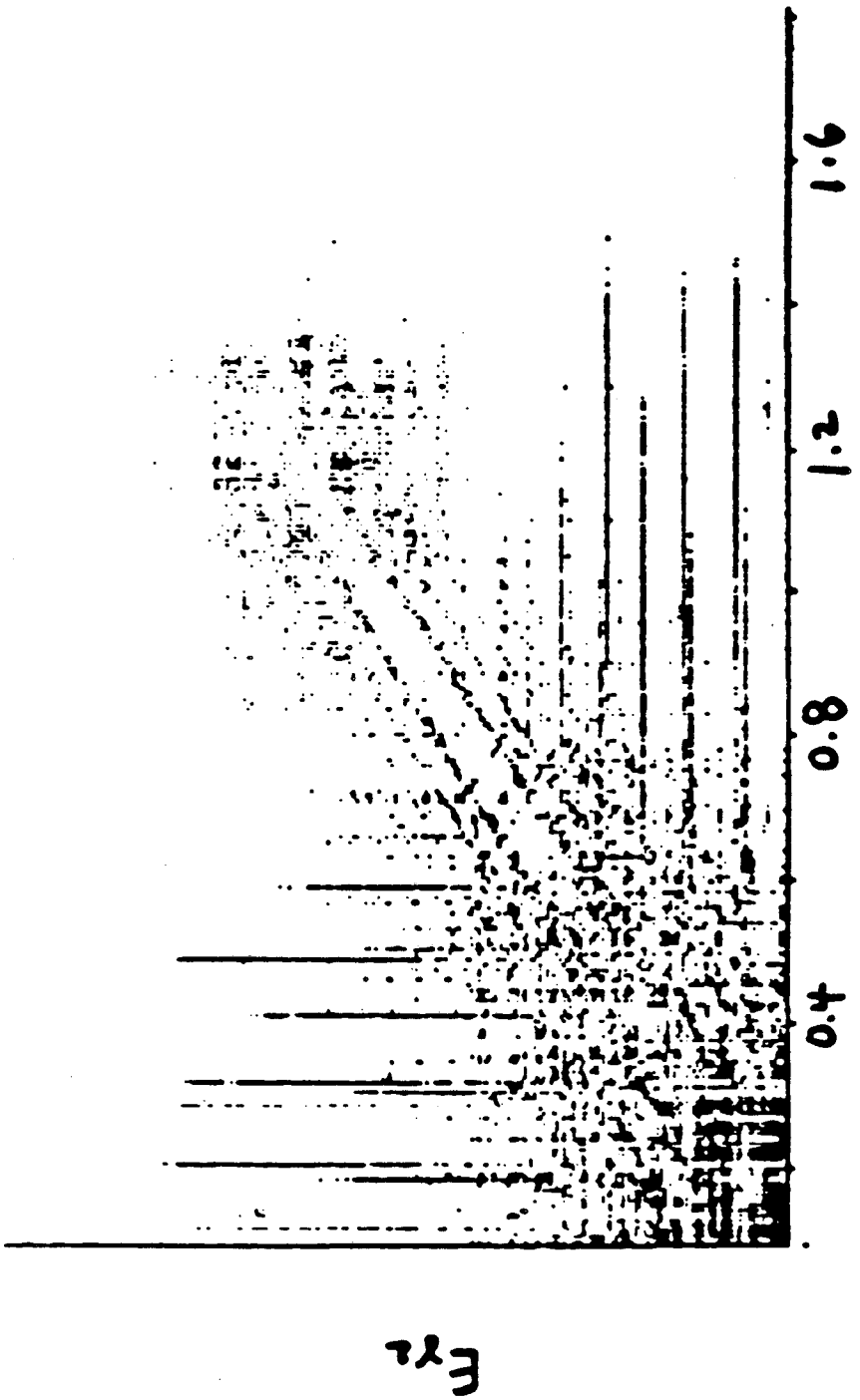

XBL 867-2683

Figure 14

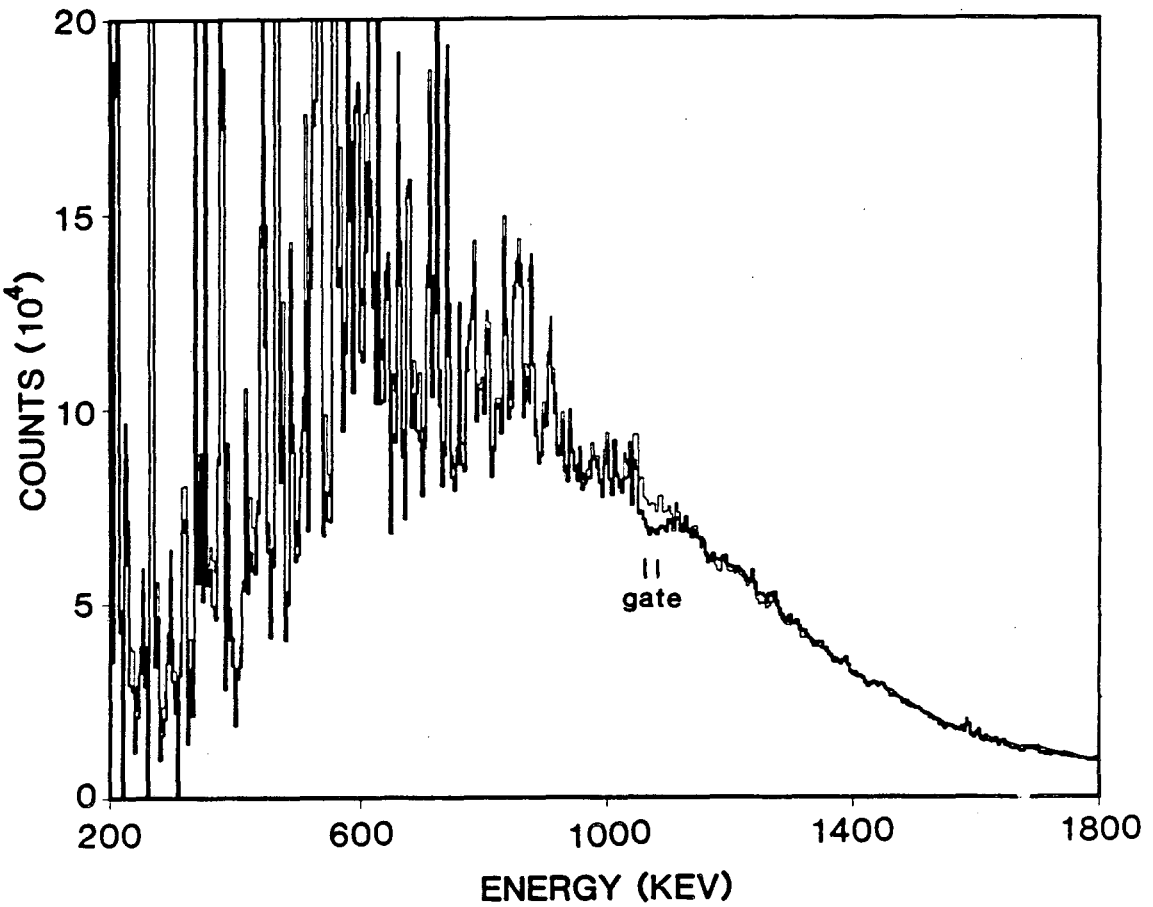

XBL 865-1834

Figure 15

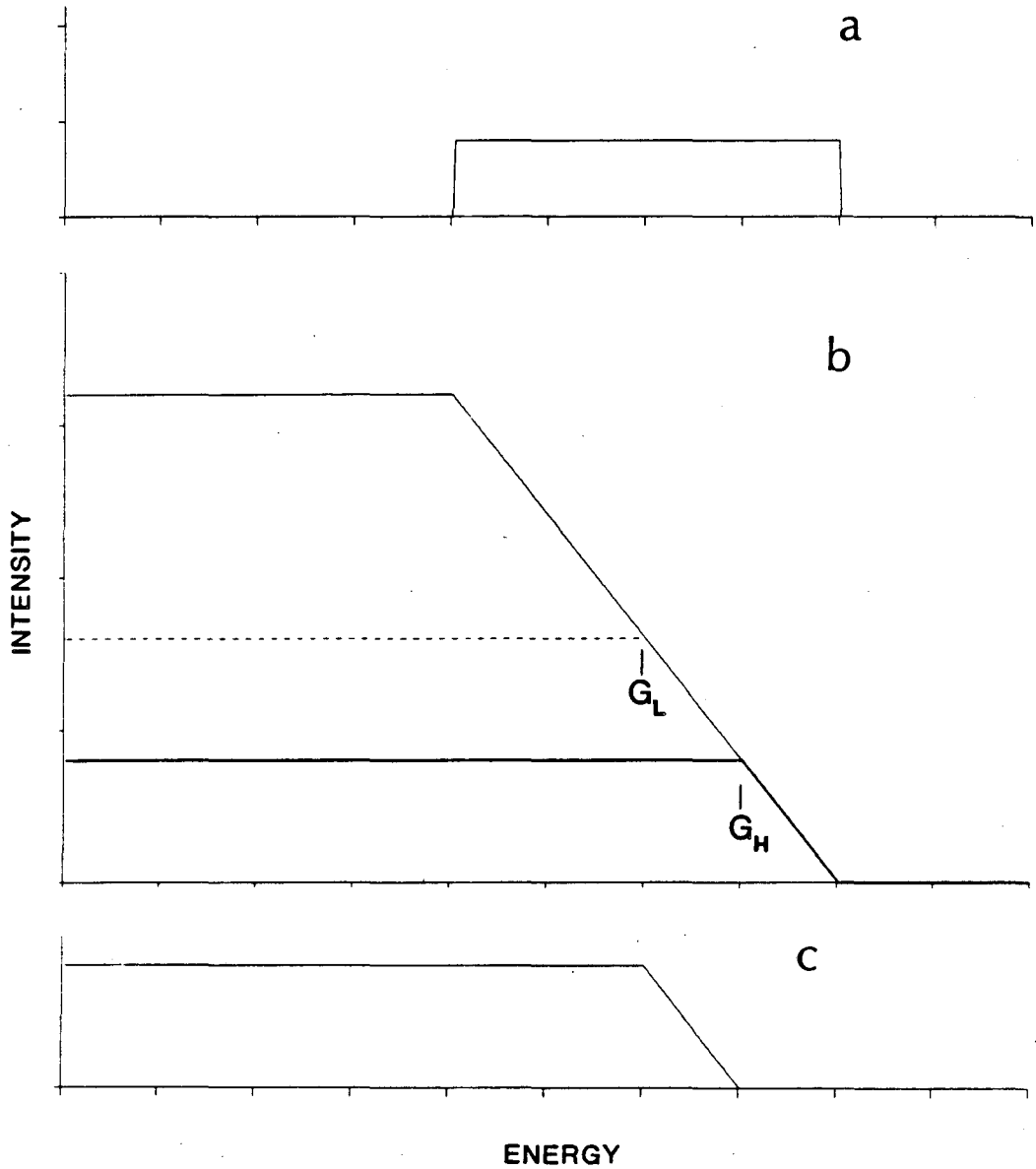

Figure 16

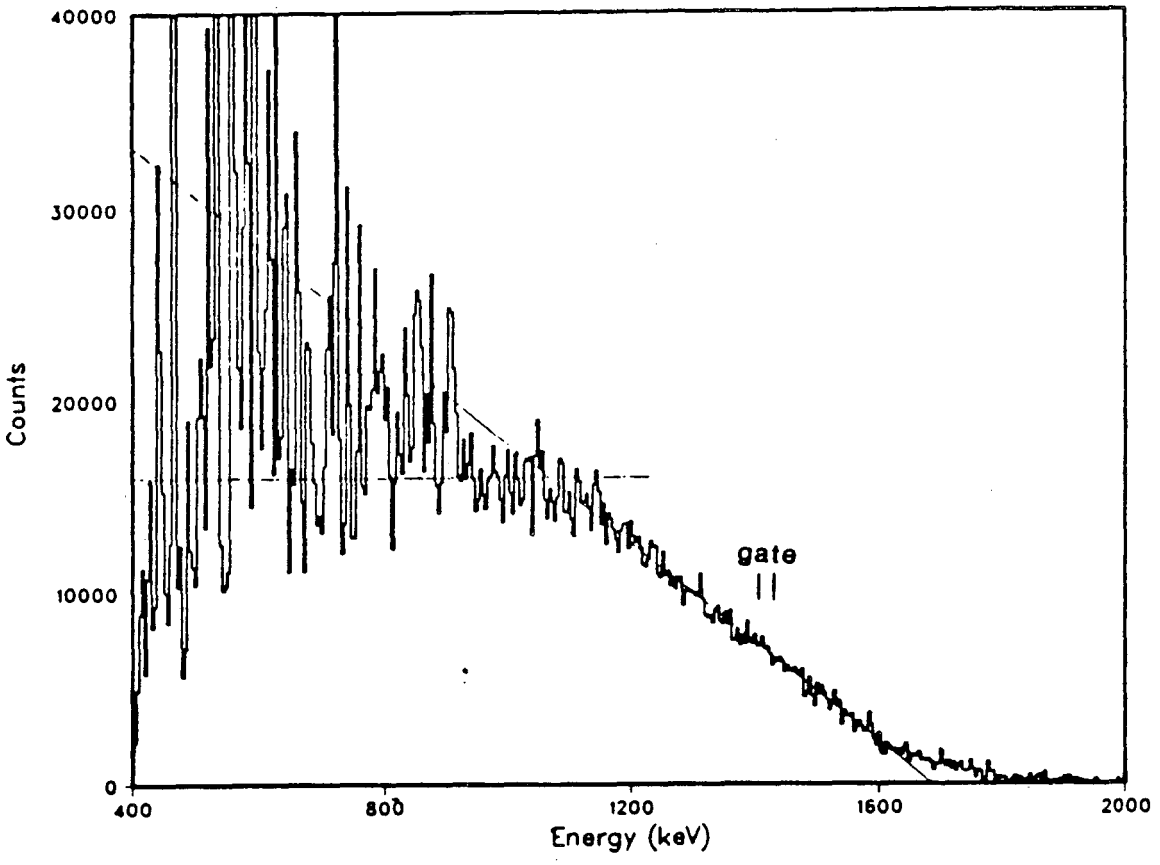

XBL 876-2522

Figure 17

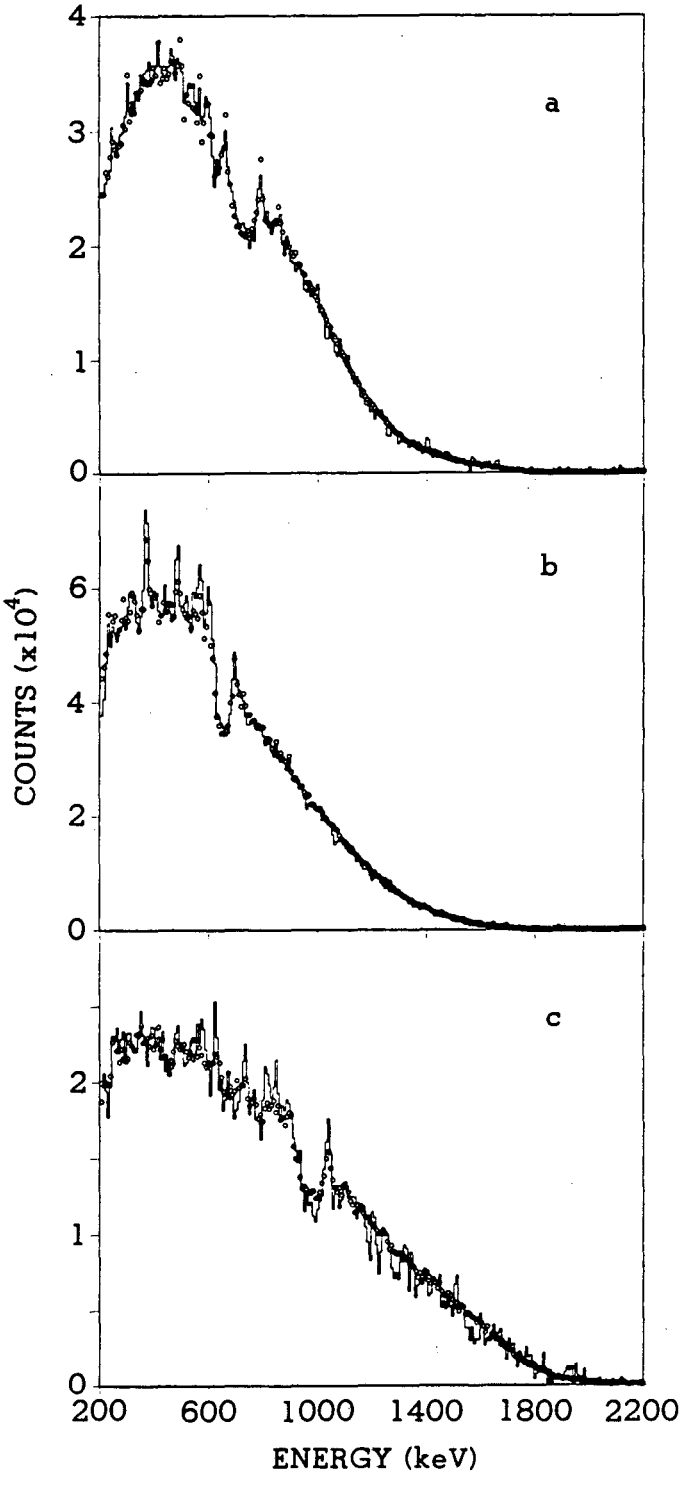
a
b
c
COUNTS (x10^4)
ENERGY (keV)
200
600
1000
1400
1800
2200
XBL 871-264

Figure 18

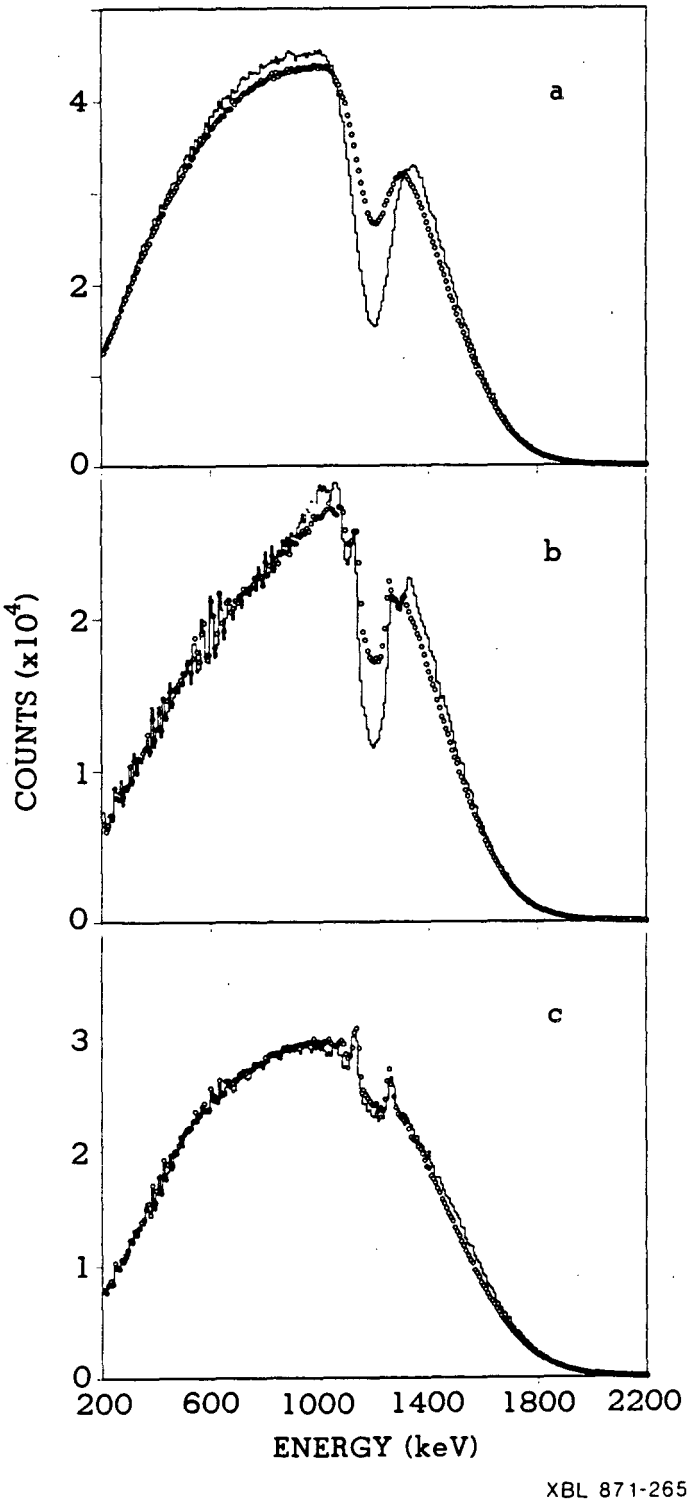
a
b
c
COUNTS (x10^4)
ENERGY (keV)
200
600
1000
1400
1800
2200
XBL 871-265

Figure 19

LAWRENCE BERKELEY LABORATORY
TECHNICAL INFORMATION DEPARTMENT
UNIVERSITY OF CALIFORNIA
BERKELEY, CALIFORNIA 94720